NEDO-24537
79NED90
CLASS I
AUGUST 1979

MARK I CONTAINMENT LONG TERM PROGRAM — DEVELOPMENT OF DOWNCOMER LATERAL LOADS FROM FULL SCALE TEST FACILITY DATA —

TASK NUMBER 7.3.2

GENERAL ELECTRIC

NEDO-24537
79NED90
Class I
August 1979

MARK I CONTAINMENT LONG TERM PROGRAM - DEVELOPMENT OF DOWNCOMER LATERAL LOADS FROM FULL SCALE TEST FACILITY DATA - TASK NUMBER 7.3.2

Prepared by EDS Nuclear Inc.
for General Electric Company

Approved: _____
G. E. Wade, Manager
Mark I Containment Design

Approved: _____
P. W. Ianni, Manager
Containment Design

NUCLEAR ENGINEERING DIVISION • GENERAL ELECTRIC COMPANY
SAN JOSE, CALIFORNIA 95125

GENERAL ELECTRIC

DISCLAIMER OF RESPONSIBILITY

Neither the General Electric Company nor any of the contributors to this document makes any warranty or representation (express or implied) with respect to the accuracy, completeness, or usefulness of the information contained in this document or that the use of such information may not infringe privately owned rights; nor do they assume any responsibility for liability or damage of any kind which may result from the use of any of the information contained in this document.

TABLE OF CONTENTS

LIST OF ILLUSTRATIONS

LIST OF TABLES

ABSTRACT

This document provides the methodology for definition of the hydraulic loads produced on the Mark I pressure suppression containment untied downcomers during a postulated loss-of-coolant accident. Resultant static equivalent lateral loads are provided for the air clearing, condensation oscillation and chugging regimes of the postulated event. This document has been prepared for the Mark I Owners as part of the Mark I Containment Program.

LIST OF ACRONYMS

DBA	Design Basis Accident
DLF	Dynamic Load Factor
FSTF	Full Scale Test Facility
IBA	Intermediate Break Accident
LOCA	Loss of Coolant Accident
OOR	Ordered Overall Range
RA	Resultant Angles
RSEL	Resultant Static Equivalent Loads
SBA	Small Break Accident
SDF	Single Degree of Freedom

1. INTRODUCTION

Task 7.3.2 of the Mark I Containment Program is to develop LOCA Loads. A subtask of this effort was the definition of downcomer lateral loads due to air clearing, condensation oscillation and chugging. This report documents the generation of these downcomer lateral loads.

The load definition is based upon test data from tests performed during 1978 in the Mark I Full Scale Test Facility (FSTF) under various LOCA conditions. The data was reduced and the loads established by EDS Nuclear Inc. under contract to General Electric Company. The methods, assumptions, justification of assumptions and results are contained herein as support for the load definition as presented in the Load Definition Report (Reference 1).

2. DESCRIPTION OF LOADING PHENOMENA

Three phases of a postulated LOCA can result in lateral loading on the downcomer. In the initial phase, the water and air expelled from the downcomer create a transient jet flow into the wetwell. This jet formation may occur asymmetrically leading to lateral reaction loads on the downcomer. This phase has been termed air clearing.

When the bulk of the drywell air has been carried over to the wetwell, essentially pure steam is forced through the downcomers into the suppression pool where the steam condenses. At the early stages of the steam blowdown phase, the steam-water interface at the vent exit is relatively stationary in time. As the blowdown proceeds and the pressure differential between the drywell and vent exit is reduced, the steam flux decreases and the steam-water interface takes on an oscillatory character. This phase is termed condensation oscillation.

At sufficiently low rates of steam flux, a more erratic motion of the steam-water interface occurs as a result of the complete and rapid collapse of the steam bubble. The asymmetric shape of the steam-water interface in the suppression pool and the bubble collapse at the ends of downcomers results in lateral loads. This phase is termed chugging.

Because of the random nature of the chugging phenomenon, there is a small but finite probability that loads on two or more downcomers will align in the same direction. This produces a resultant loading on the vent header which is larger in magnitude than the maximum load observed to act on a single downcomer. When two or more downcomers chug sychronously the event has been referred to as pool chug synchronization.

3. TEST FACILITY

As a part of the Mark I containment program, a test program was defined and implemented to obtain full scale condensation oscillation and chugging data.

In the fall of 1976, preliminary specifications for the test program were established. Construction of the facility was initiated in 1977 and completed in early 1978. Shakedown testing began in March, 1978, and the ten test program was completed in August, 1978.

3.1 FACILITY DESCRIPTION

The FSTF was designed to simulate behavior of the Mark I containment system in response to LOCA conditions. The Monticello plant suppression chamber (wetwell) was selected as the basis for the reference geometry for the test facility. The considerations used in specifying the requirements for the facility and the bases for selection of Monticello as the reference plant are contained in Reference 2.

The facility configuration is shown in Figure 3-1 and 3-2. The wetwell is shown in Figure 3-3 and the vent system detail is shown in Figure 3-4. The wetwell is prototypical of one Monticello bay between the vent pipes and contains eight downcomers. The internal vent header and downcomers are also prototypical of Monticello except that the downcomers were shortened to a reduced submergence (3 ft. 4 in.) to reflect the direction of the containment program toward mitigation.

3.2 TEST CONDITIONS

Tests were run over a range of conditions representative of postulated LOCA's for the Mark I Containment. The test parameters varied were the blowdown size and type (liquid and steam), the downcomer submergence, the initial pool

temperature, the final free space pressure, and the vent air content. The FSTF test matrix is shown in Table 3-1.

Several changes were made to the facility as the testing program progressed. These changes are summarized as follows.

1. Following test number 3 the ring header protector (deflector) and tension-only (prototypical to Monticello) tie straps between downcomer pair 7 and 8 were added.

2. Following test number 9 three ring header stiffeners and compression/tension bracing between downcomer pairs 1 & 2, 3 & 4 and 5 & 6 were added.

3. A plate was inserted to inactivate the vacuum breaker for test number 10. This plate was removed prior to test number 7.

4. Following test number 10 perforations to the stand pipe in the drywell were made.

5. Following test number 7 the tie strap between downcomer pairs 5 & 6 was removed along with the two adjacent vent header stiffeners.

The reasons for these changes are documented in Reference 2.

3.3 INSTRUMENTATION

For the purpose of downcomer lateral load definition, data from orthogonal bending bridges on downcomers 6 and 8 were recorded for all the tests. The location of the bending bridges are shown in Figure 3-4 to be midway between the vent header/downcomer junction and the mitered bend on the downcomer.

962069

Data from each of these bending bridges was recorded for all ten tests with a sampling rate of approximately 1000 samples per second with a 13 bit resolution.

Table 3-1

FSTF TEST MATRIX

Test Number[a]	Break Size	Break Type	Initial Conditions: Submergence	Initial Conditions: T_{ww}	Initial Conditions: P_{ww}	Chugging Occurred	Downcomer[d] Configuration 1-2	3-4	5-6	7-8
1	IBA	Steam	3 ft 4 in	70°F	0 psig	yes	1	1	1	1
2	IBA/DBA	↓	↓	↓	↓	no	1	1	1	1
3	IBA	Liquid	↓	↓	↓	no	1	1	1	1
4	↓	Steam	↓	↓	5 psig	yes	1	1	1	3
5	↓	↓	↓	120°F	0 psig	no	1	1	1	3
6	↓	↓	1 ft 6 in	↓	↓	no	1	1	1	3
9	↓	↓	4 ft 6 in	70°F	↓	yes	1	1	1	3
10[b]	↓	↓	3 ft 4 in	↓	↓	yes	2	2	2	3
7	DBA	↓	↓	↓	↓	no	2	2	2[c]	3
8	↓	Liquid	↓	↓	↓	no	2	2[c]	1	3

Downcomer Configuration:

1 - Free (untied)

2 - Tension/compression bracing (pipe)

3 - Tension-only tie strap (prototypical)

(a) Tests listed in order of performance

(b) Air sensitivity test performed with vacuum breaker replaced with rupture disc

(c) Tie-bar instrumented for axial load

(d) See Figure 3-4 for numbering of downcomers

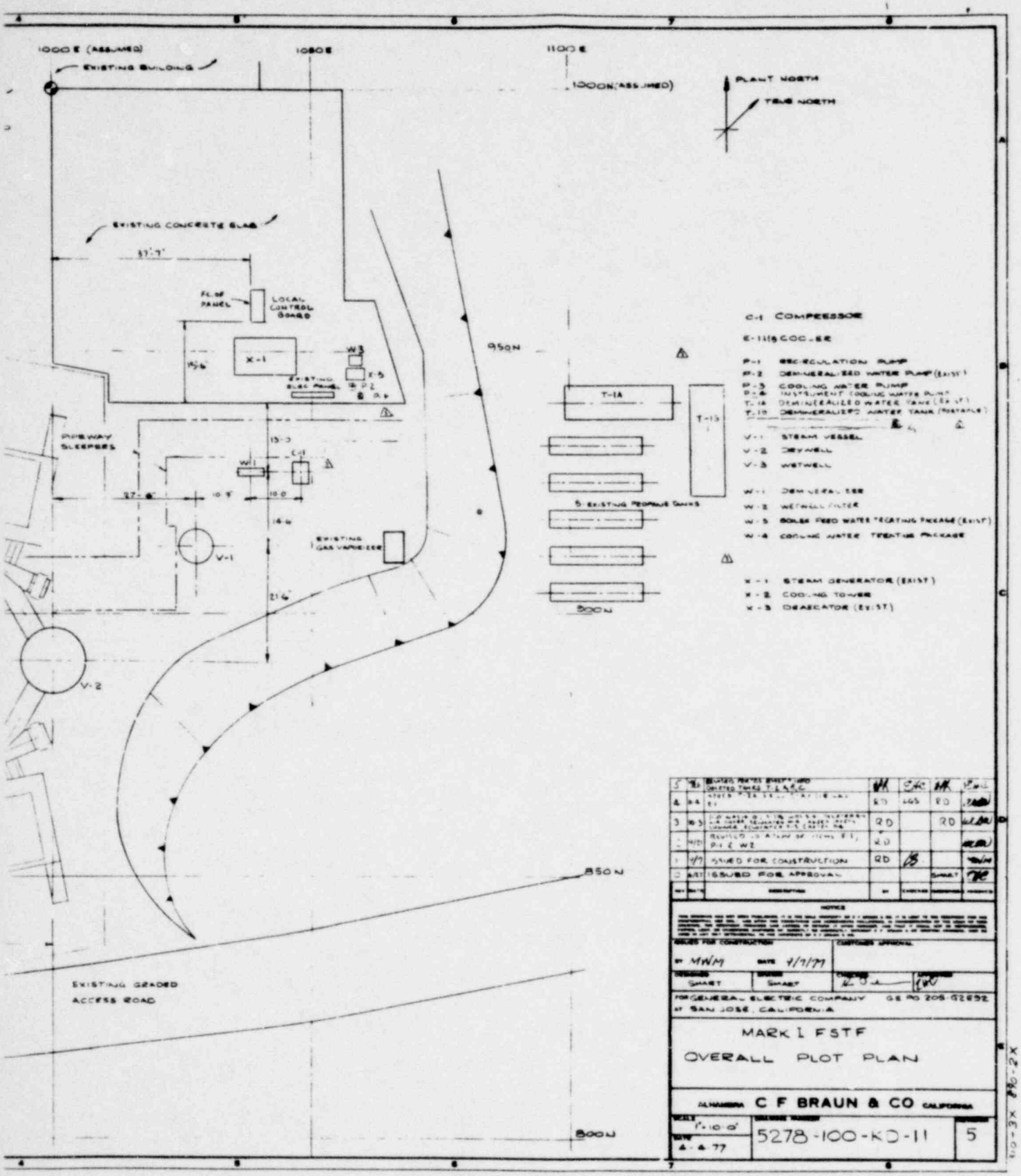

Figure 3-1. Mark I FSTF - Overall Plot Plan

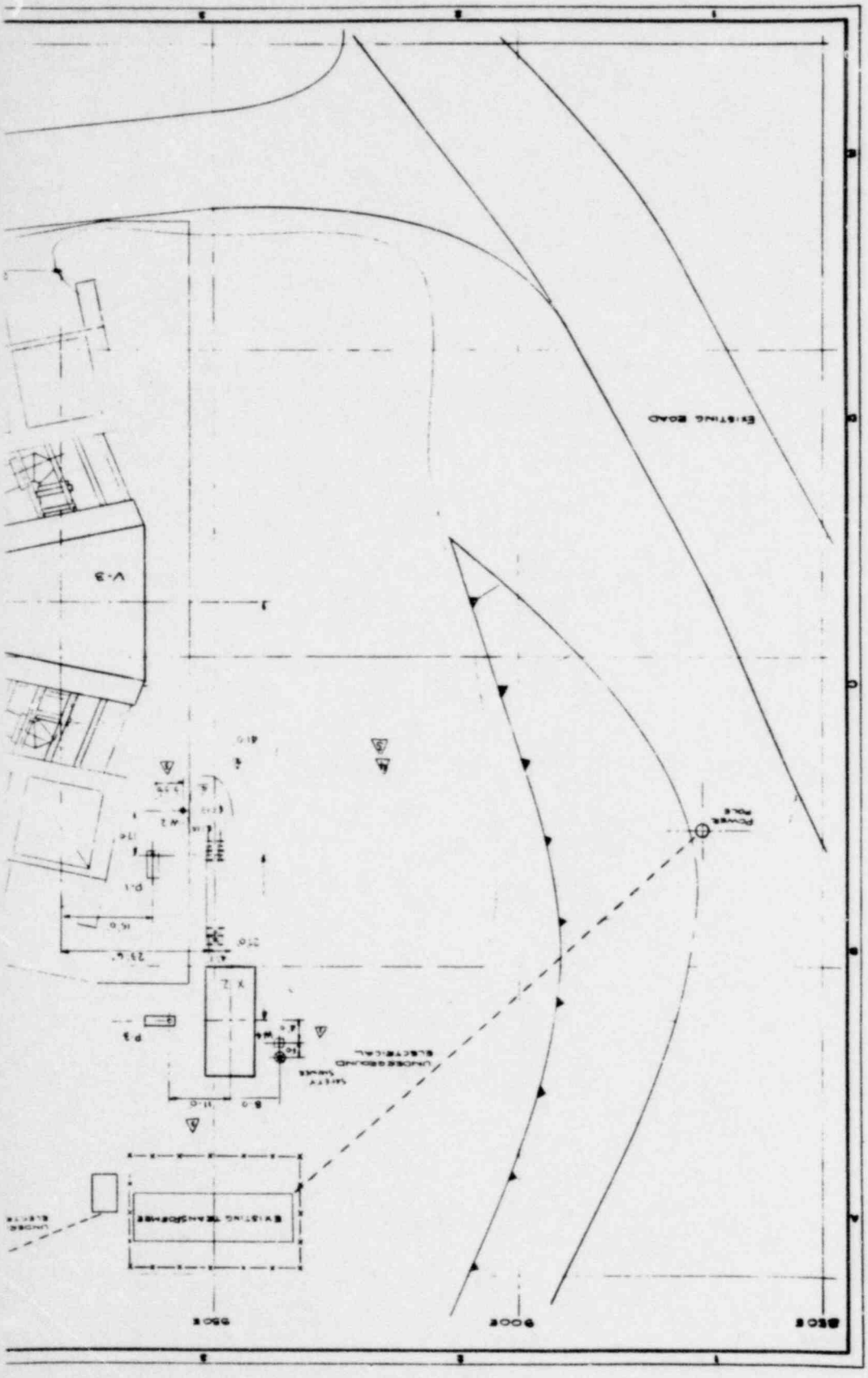

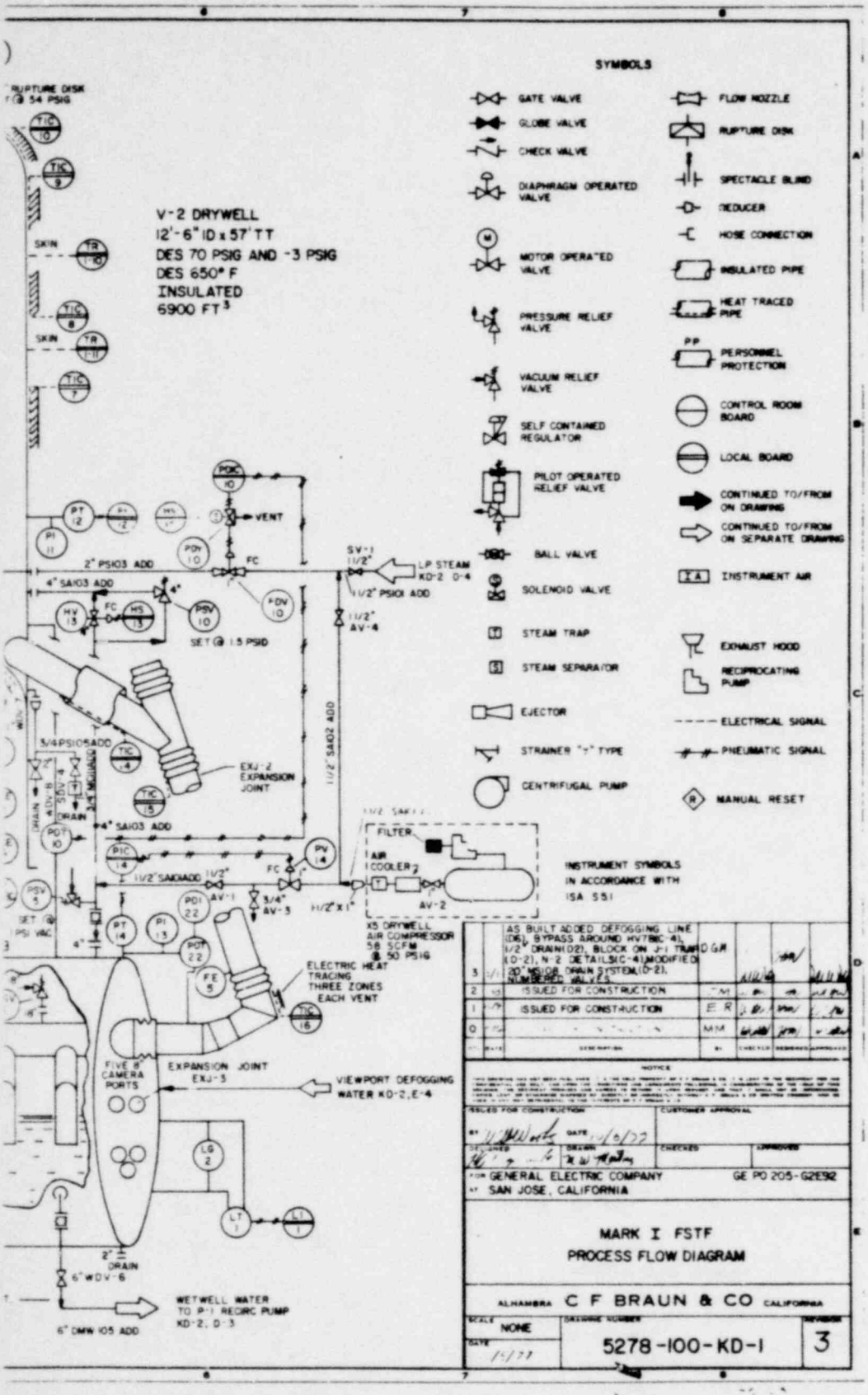

Figure 3-2. Mark I FSTF - Process Flow Diagram

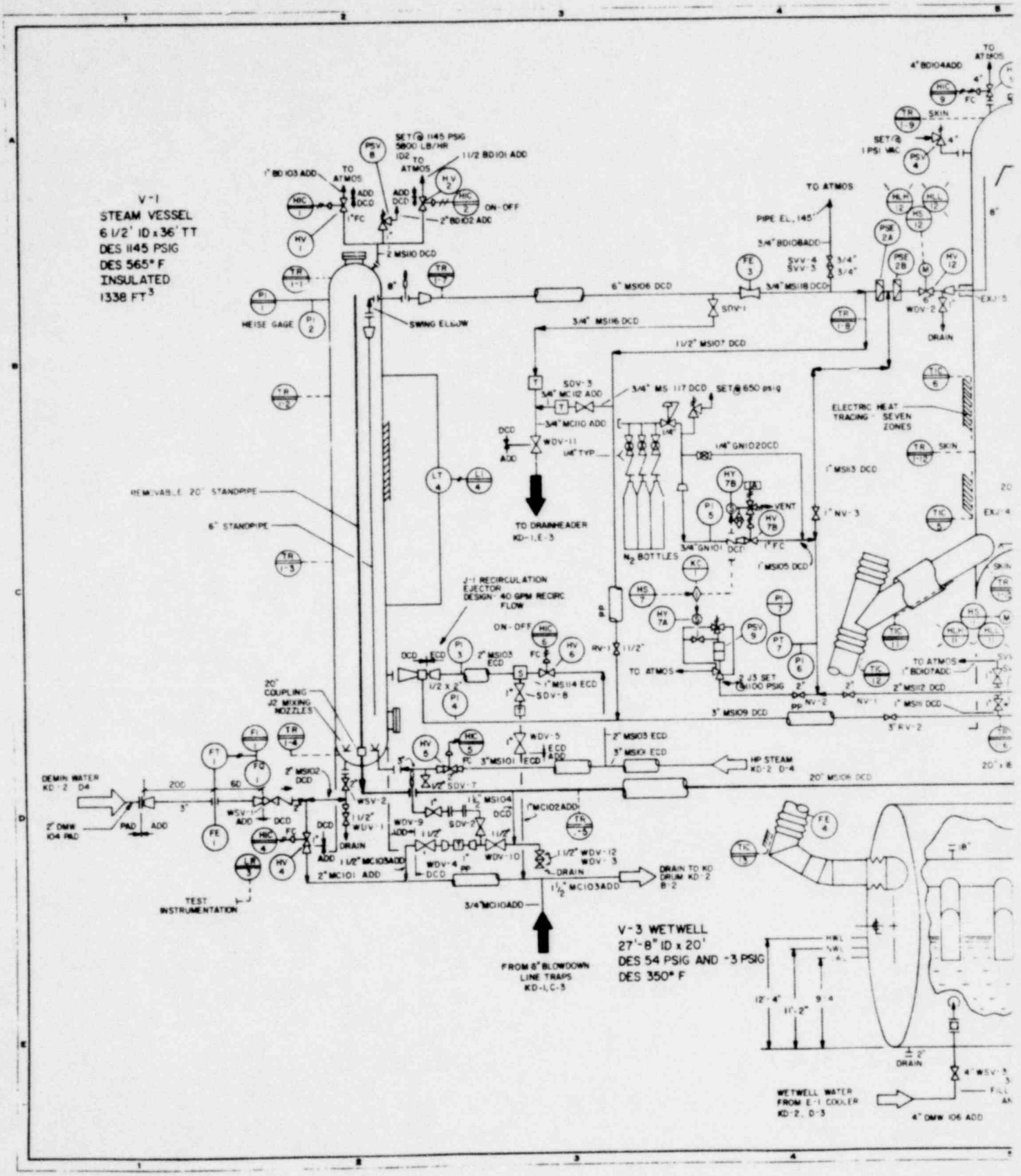

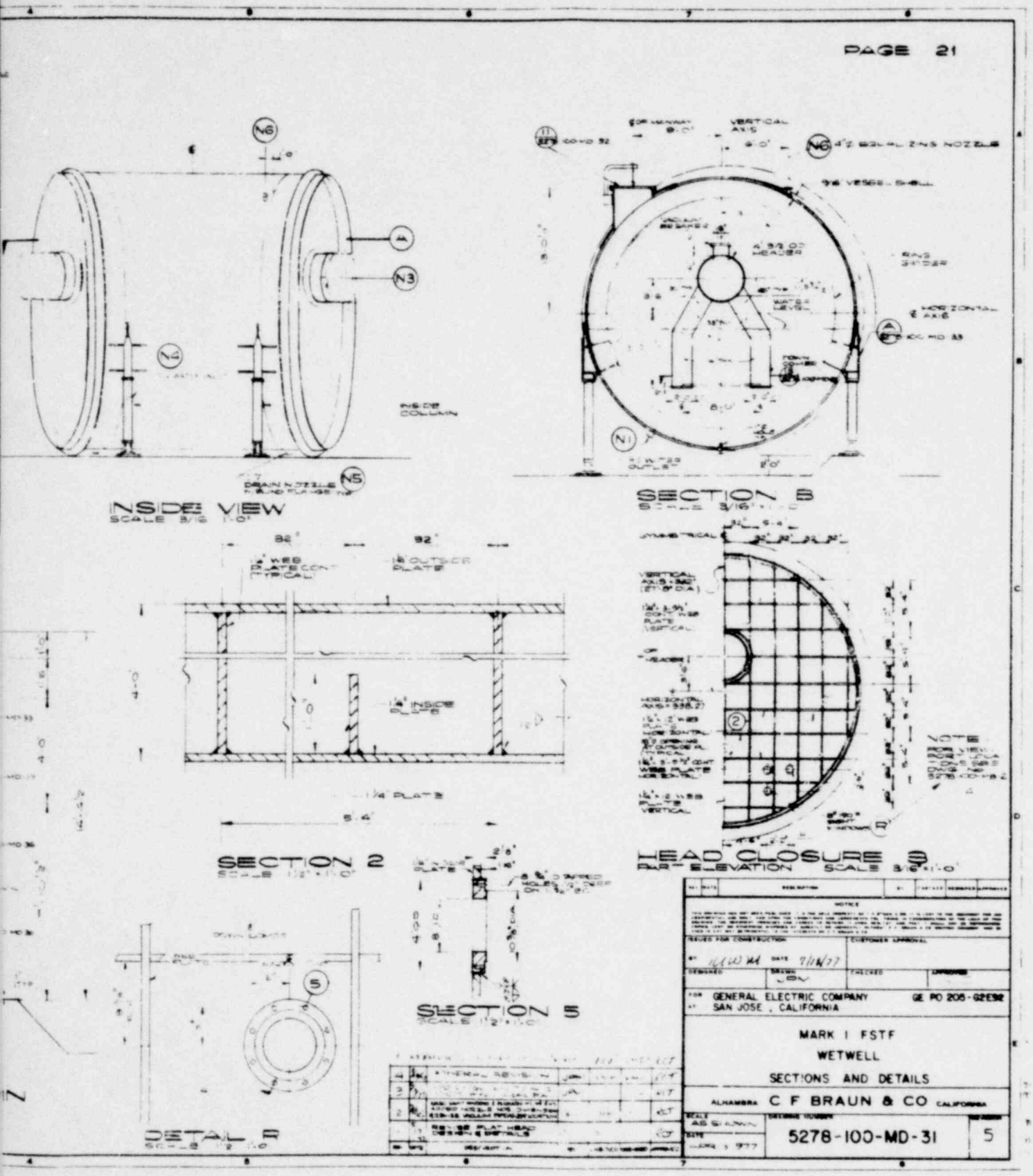

Figure 3-3. Mark I FSTF - Wetwell Sections and Details

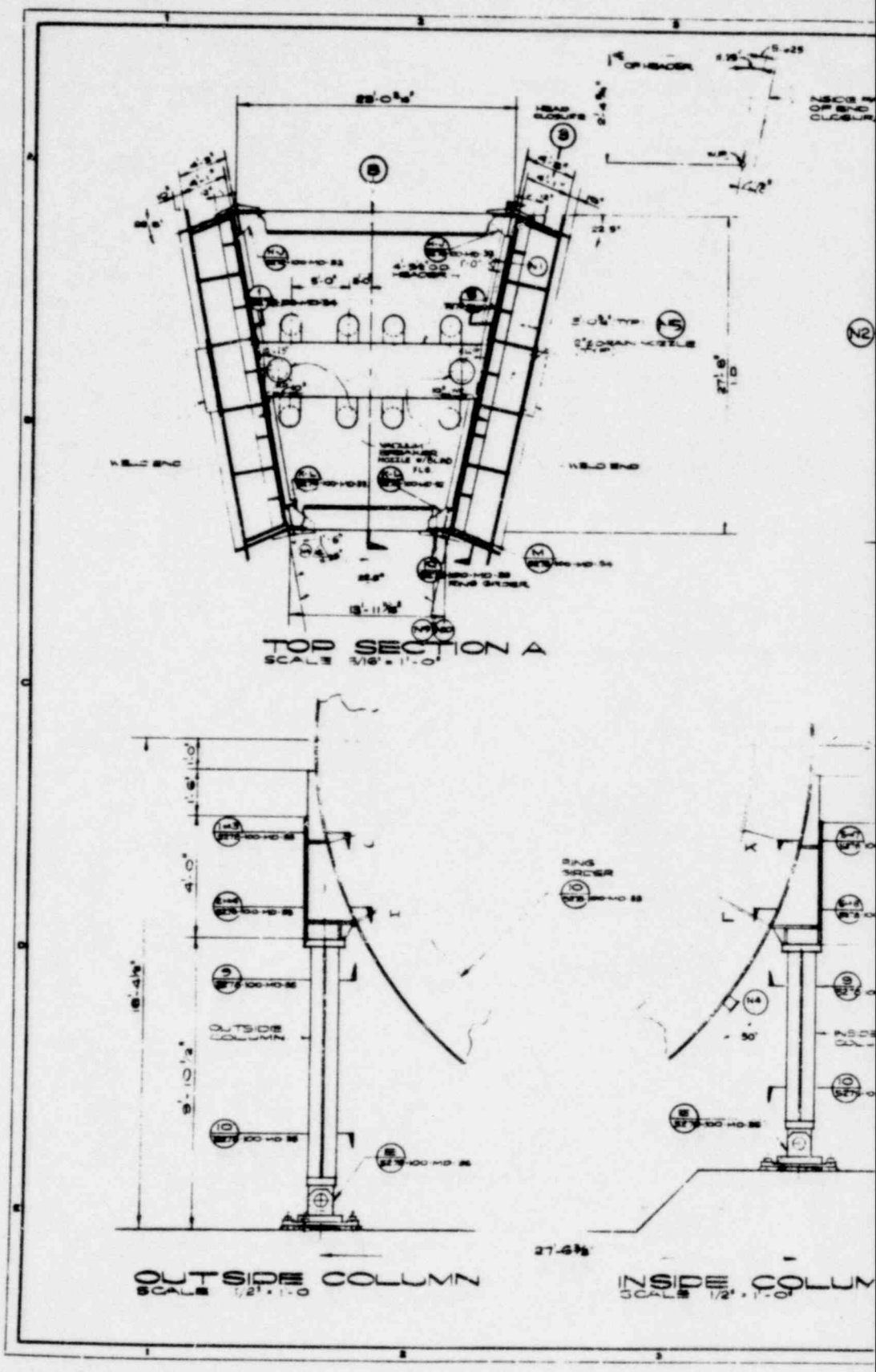

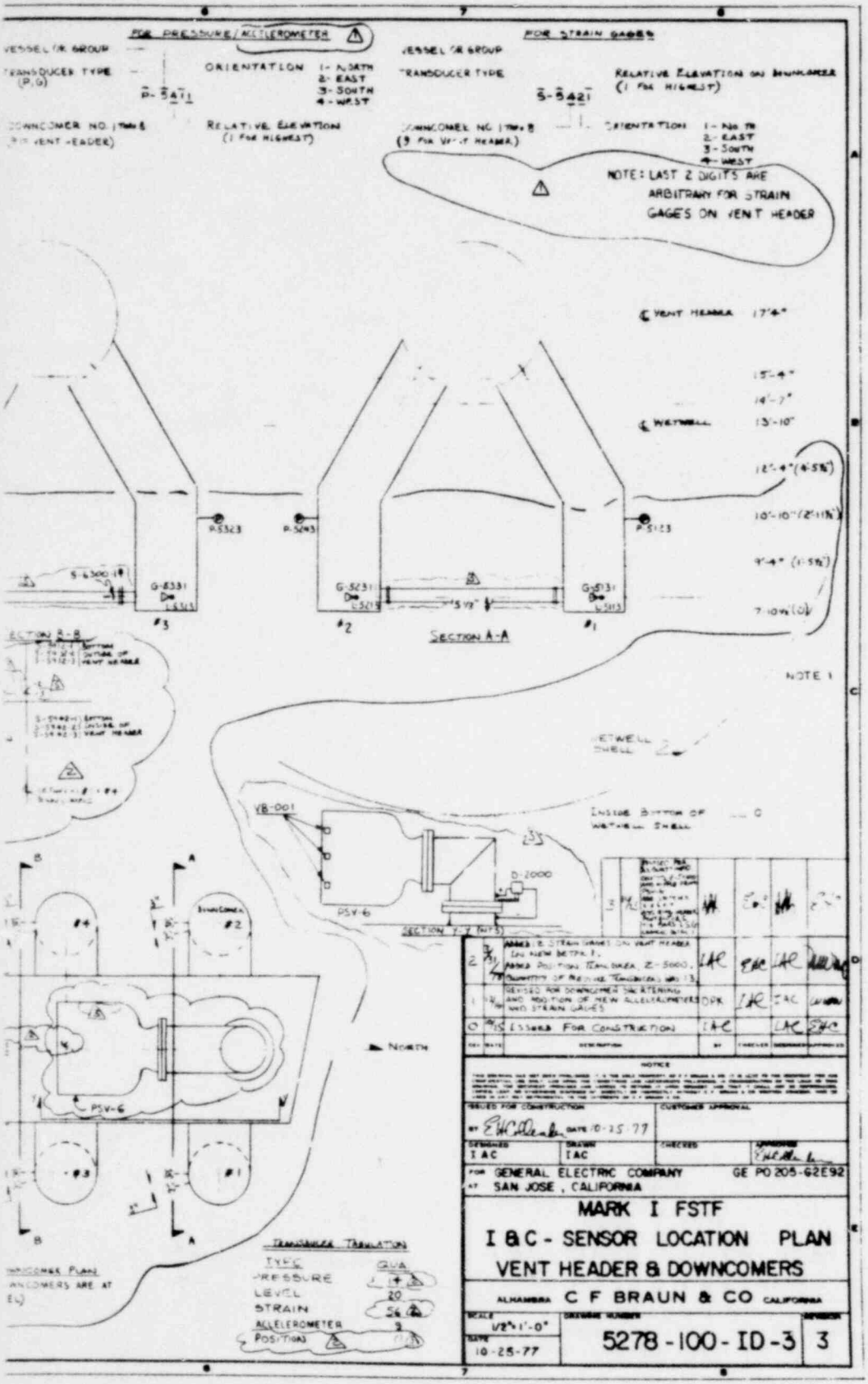

Figure 3-4. Mark I FSTF - Vent Header and Downcomers Sensor Location Plan

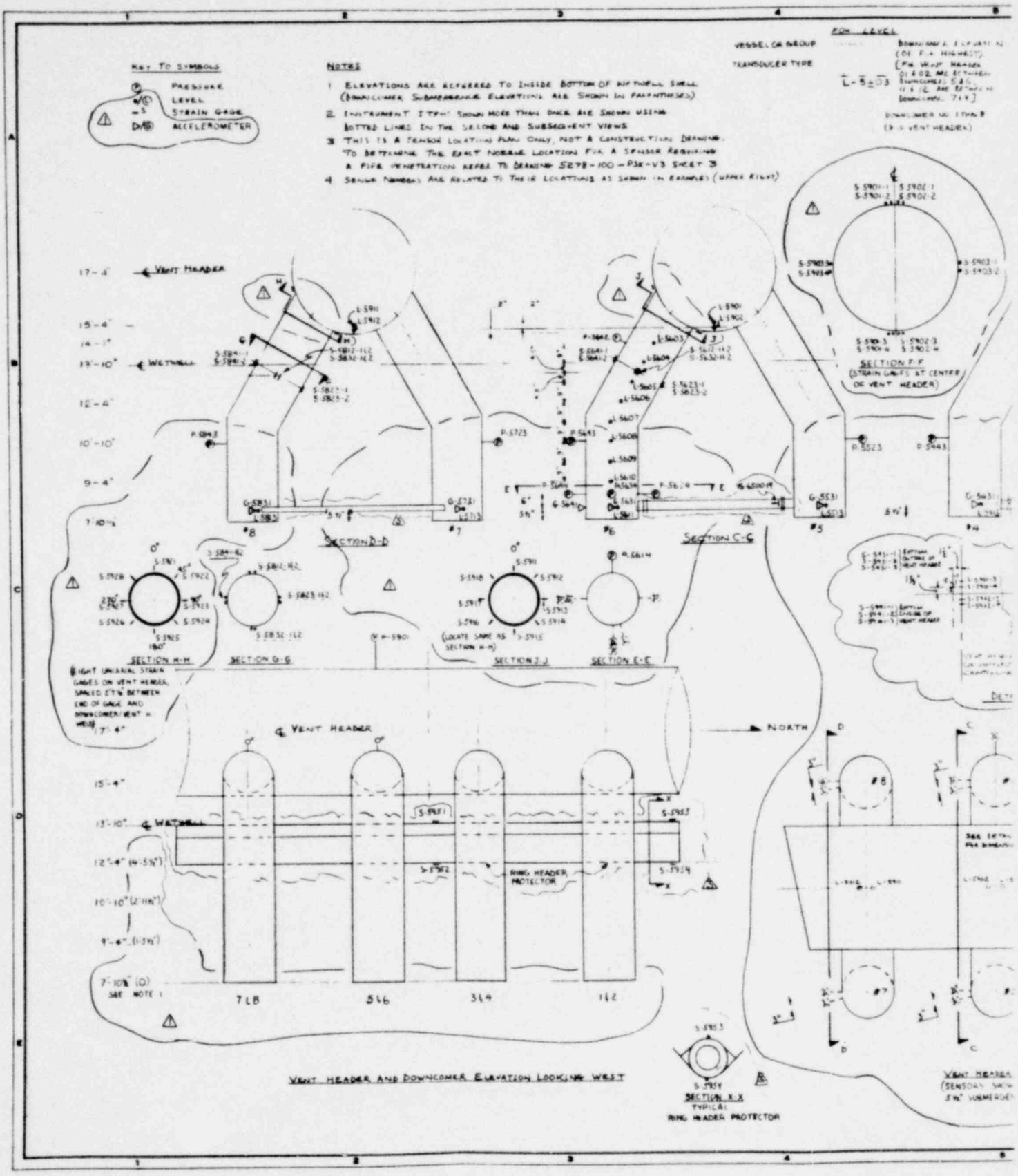

4. METHODOLOGY FOR DETERMINING DOWNCOMER LATERAL LOADS

The load definition methodology is based upon the measured response of downcomer numbers 6 and 8 in the FSTF (Figure 3-4) subjected to LOCA testing for various conditions.

The FSTF downcomer lateral loads are defined as Resultant Static Equivalent Loads (RSEL) which, when applied statically to the end of the downcomer, will reproduce at any given time the measured bending response near the downcomer/vent header junction. The RSEL were obtained from the measured downcomer bending moments using conversion factors determined from static calibration tests performed on the downcomers (Appendix A). These RSEL are, therefore, an actual representation of the structural-hydrodynamic interaction which occurs during a LOCA.

The maximum design loads for individual plants are obtained by scaling the maximum RSEL from the FSTF. The scaling factors are derived on the basis of a comparison of the dynamic characteristics of the downcomers of the individual plants and the FSTF.

Additionally, the number of RSEL reversals during the FSTF condensation oscillation and chugging phases were counted and presented in the form of RSEL reversal histograms. Since the loads may be oriented in any arbitrary lateral direction, these histograms were obtained for each of eight diametrically opposed angular sectors around the downcomer end. The FSTF RSEL reversal histograms are scaled into a plant-unique set of histograms by first scaling the maximum RSEL reversal on the same basis as was done for the maximum design loads. Then the number of RSEL reversals are scaled by the ratio of the condensation oscillation or chugging durations specified for the plants to that of the FSTF. For fatigue evaluation of the downcomer/vent header junction, the plant-unique set of RSEL reversals must be converted to a set of stress reversals at the downcomer/vent header junction which result from application of the RSEL reversals.

During the chugging phenomenon lateral loads, i.e., RSEL are imposed on the ends of the downcomers which are random in both magnitude and direction. Because of the random nature of these chugging forces, there is a small but finite probability that the RSEL on two or more downcomers will align in the same direction to produce a resultant loading which is larger in magnitude than the maximum RSEL observed to act on a single downcomer. When two or more downcomers chug synchronously the event has been referred to as pool chug synchronization.

During the condensation oscillation phenomenon, the resultant lateral or radial loads on the vent system were negligible because the downcomer pairs were observed to respond essentially out-of-phase in their plane. In addition, the net loads observed along the axis of the vent header were smaller than those predicted for pool chug synchronization.

4.1 ASSUMPTIONS

A number of assumptions are involved in the load definition methodology. They are each presented and are followed by their technical justification.

1. The vent header and downcomers can be considered rigid when compared to the flexible downcomer/vent header junction and therefore the downcomer will respond dynamically in any given direction as a single-degree-of-freedom (SDF) system.

   JUSTIFICATION

   A comparison was made of the downcomer/vent header systems for all Mark I plants. This comparison verified that the downcomers are at least 50 times more stiff than their junctions except for Browns Ferry where it is 12 times as stiff. These results are summarized in Table 4-1. Therefore, the downcomer responds dynamically in any given direction as a single degree of freedom system. This assumption has been verified by the following analytical study.

A finite element model using beam elements and a rotational boundary element, i.e. torsional spring, was used to model the downcomer/vent header structure, as shown in Figure 4-1. The material and structural properties used for the FSTF downcomer finite element model were those shown in Table 4-2. The stiffness of the boundary element was selected in order that the model stiffness matched the measured stiffness obtained from the FSTF static calibration tests described in Appendix A. The stiffness value selected was confirmed by applying a static load (F) at the tip of the downcomer and comparing the resultant tip displacement with that of the calibration tests.

For dynamic analyses of the FSTF downcomer/vent header structure, added mass effects due to the water were also included. The added mass used was taken as one-third of the fluid mass displaced by a closed cylinder of dimensions equal to the submerged portion of the downcomer. This added mass value was derived such that the analytically determined natural response of the downcomer matched the observed FSTF downcomer response. The appropriate added mass value was added to the beam elements representing the submerged portion of the downcomer as shown in Figure 4-1.

The dynamic behavior of the downcomer/vent header structure subjected to a simulated chugging load was studied to determine whether the SDF assumption was valid and therefore that the higher modes do not contribute significantly to the response. Modal analyses using four modes and one mode were performed. It is seen from Figure 4-2 that the resulting downcomer response, i.e., tip displacement, was not significantly affected by eliminating the higher modes, thus confirming the SDF assumption.

2. The lateral hydraulic loads experienced by the FSTF downcomers during air clearing, condensation oscillation and chugging are representative

of the loads that would be experienced by other Mark I downcomers for the same conditions. Also the FSTF RSEL reversal histograms are representative of an actual plant behavior over the same duration. Thus, for the fatigue evaluation of an individual plant's downcomer, the FSTF RSEL reversal histogram data must be scaled by the ratio of the condensation oscillation or chugging durations in the plant to those respective durations simulated in the FSTF.

JUSTIFICATION

The magnitude and frequency of lateral loads are principally controlled by the geometry of the vent system, blowdown mass flux, air content and pressure and temperature conditions of the wetwell. The significant dimensions of the wetwell, ventline, downcomer and operating pressure and temperature of the wetwell for the FSTF and the Mark I plants are listed in Table 4-3.

It can be seen from Table 4-3 that the FSTF typically represents the Mark I plants except for Duane Arnold which has only about one half of the number of downcomers. The FSTF simulates a 22 1/2° segment of a typical wetwell. Because of the vent line arrangement in the FSTF, two vent lines are equivalent to one vent line of an actual plant. Although the length and arrangement of the FSTF vent lines are not the same, the total flow resistance (K factor) of the vent system was simulated to be the same.

The drywell volume per downcomer for the FSTF was much lower than the actual Mark I plants. Since a smaller wetwell and drywell volume would yield a higher pressure amplitude and frequency, the FSTF results would be conservative.

Because the FSTF is representative of actual Mark I plants, with the exception of Duane Arnold, the load phenomena and magnitude are representative of actual plants.

3. The dynamic portion of the condensation oscillation loads can be approximated as sinusoidal in nature and the chugging loads can be approximated as triangular pulse loads.

JUSTIFICATION

As indicated by the typical bending bridge strain traces shown in Figures 4-3 and 4-4 for FSTF test number 1, the condensation oscillation loads are continuous and sinusoidal and the chugging loads are triangular pulse loads.

4. The load definition procedure is applicable for loadings where the measured bending strains on the downcomer remain within the elastic range.

JUSTIFICATION

For downcomers comprised of A36 steel having a yield stress of 36 ksi and an elastic modulus of 30×10^3 ksi, the resulting yield strain for the material is 1200 μ in/in. Figure 4-5 shows sample portions of the measured bending strain responses for downcomer numbers 6 and 8 from the condensation oscillation region of FSTF test no. 8. The test no. 8 condensation oscillation RSEL were the most significant lateral loads determined from the series of FSTF tests, and the associated bending strains are observed in Figure 4-5 to remain well within the elastic range.

5. The loading on any given downcomer as determined from the measured downcomer bending response is predominantly due to a chug occurring on that downcomer. The effect that chugs on neighboring downcomers have on the measured bending response can be neglected.

JUSTIFICATION

Visual inspection of the bending bridge strain gauge data for FSTF downcomer numbers 6 and 8 determined that the response for one downcomer was small when adjacent downcomers chugged. Figure 4-6 shows a typical interaction response during chugging. For a chug occurrence at 211.5 seconds on downcomer number 6 it is seen that the resulting response at downcomer number 8 is insignificant. The structural-hydrodynamic phenomenon which takes place during multi-vent chugging is however, inherent in the FSTF data and the RSEL thus determined include this effect.

6. The load definition procedure has been developed for, and is directly applicable to downcomers free of structural ties. For Mark I plants containing structural ties between each downcomer pair comparable in stiffness to the 2-in. by 1/4 in. tie straps of the FSTF, the plant-unique condensation oscillation loads may be conservatively reduced by factors of 0.85 for the IBA and 0.75 for the DBA. No load reduction is specified for chugging lateral loads.

JUSTIFICATION

The condensation oscillation reduction factors of 0.85 and 0.75 for the IBA and DBA loads, respectively, were derived based upon actual FSTF test comparisons between tied and untied downcomer pairs. From the FSTF test summary presented in Table 3-1, FSTF tests 4, 5, 6 and 9 which were representative of an IBA condition all had downcomer number 6 untied and downcomer number 8 tied with a tension-only prototypical tie strap. A similar configuration existed for the FSTF DBA test no. 8. Both downcomer numbers 6 and 8 from these tests were analyzed to determine the amount by which the structural tie reduces the maximum RESEL.

A comparison of the maximum RSEL for tied and untied downcomers from these IBA and DBA tests is shown in Table 4-4. The ratio of the tied

to untied IBA RSEL was observed to vary from 0.62 to 0.85 for condensation oscillation. Similarly, a ratio of 0.61 was observed for the condensation oscillation regime of FSTF DBA test no. 8. IBA and DBA condensation oscillation reduction factors of 0.85 and 0.75, respectively, were therefore selected as conservative representative values.

For determination of chugging lateral loads on tied downcomers, the load definition procedure may be used without introducing additional conservatism, since the chugging loads observed in the FSTF were directionally random in nature. This conclusion is supported by the comparison of maximum RSEL for tied and untied downcomers for the chugging portions of FSTF test nos. 4 and 9. As shown in Table 4-4, the ratio of tied to untied RSEL from test nos. 4 and 9 are 0.87 and 1.02, respectively.

7. When considering the chug synchronization load, all downcomers experience chugging in phase and the magnitude and direction of the chugging load on a downcomer is statistically independent from all other downcomers.

JUSTIFICATION

Observation of the FSTF data indicates that chugging load magnitude and direction are both independent of the downcomer upon which the loads were measured. This is confirmed by the scatter diagram shown in Figure 4-7, which shows peak chug magnitude versus direction for downcomer numbers 6 and 8 of FSTF test no. 1. Since these downcomers were the only two instrumented for downcomer lateral loads and were independent, it is reasonable to assume that they are representative of any given number of such downcomers.

Chugs occurring simultaneously or in phase were not observed in the FSTF data but was introduced as a simplifying assumption. Neglecting the random occurrence of chugs is a conservative assumption.

4.2 PEAK LOAD CALCULATION

The most noteworthy feature of the downcomer load definition is that it is based on the measurement of significant structural response to the lateral load, rather than the load itself. It is this feature that permits the load to be defined in a form that can be used together with static analyses.

The instrumented downcomers of the FSTF have a pair of bending bridges installed just below the downcomer/vent header intersection as shown in Figure 3-4 and schematically in Figure 4-8. These bending bridges are initially calibrated by applying static loads to the downcomer end in directions corresponding to P_{NS} and P_{EW}, and the calibration constants so determined are used to establish the following relationship:

$$\begin{Bmatrix} P_{NS} \\ P_{EW} \end{Bmatrix} = \begin{bmatrix} K_{NN} & K_{NE} \\ K_{EN} & K_{EE} \end{bmatrix} \begin{Bmatrix} e_{NS} \\ e_{EW} \end{Bmatrix} \tag{4.1}$$

where:

e_{NS} = Measured bending strain in the North-South direction, in/in. Compression at North side is positive.

e_{EW} = Measure bending strain in the East-West direction, in/in. Compression at East side is positive.

K_{NE}, K_{EE} = Input constants for calculation of equivalent lateral force in the East-West direction.

K_{NN}, K_{EN} = Input constants for calculation of equivalent lateral force in the North-South direction.

P_{NS} = Equivalent lateral force on the end of the downcomer in the North-South direction, lbs. North is positive.

P_{EW} = Equivalent lateral force on the end of the downcomer in the East-West direction, lbs. East is positive.

The input or calibration constants (K) are determined from the static calibration tests described in Appendix A. These constants are determined by first calculating the flexibility coefficients (F) and then converting them to stiffness or input coefficients as follows:

F_{NN} is the bending strain in the North-South direction due to unit lateral force in the North direction, i.e., slope of line drawn through calibration data as shown in Figure 4-9(a).

F_{NE} is the bending strain in the East-West direction due to unit lateral force in the North direction, i.e., slope of line as shown in Figure 4-9(b).

F_{EN} is the bending strain in the North-South direction due to unit lateral force in the East direction, i.e., slope of line as shown in Figure 4-9(c).

F_{EE} is the bending strain in the East-West direction due to unit lateral force in the East direction, i.e., slope of line as shown in Figure 4-9(d).

then

$$K_{NN} = \frac{F_{EE}}{D}$$

$$K_{NE} = \frac{-F_{NE}}{D}$$

$$K_{EN} = \frac{-F_{EN}}{D}$$

$$K_{EE} = \frac{F_{NN}}{D}$$

where $D = F_{NN} F_{EE} - F_{NE} F_{EN}$

The equivalent lateral forces in the North-South and East-West directions are then combined into resultant static equivalent loads (RSEL) and resultant angles (RA) as follows:

$$RSEL = \sqrt{P_{EW}^2 + P_{NS}^2}$$

$$RA = TAN^{-1}\left(\frac{P_{EW}}{P_{NS}}\right) \quad IF \quad P_{EW} > 0, \; P_{NS} > 0$$

$$= TAN^{-1}\left(\frac{P_{EW}}{P_{NS}}\right) + 180^\circ \quad IF \quad P_{EW} < 0, \; P_{NS} < 0$$

$$= TAN^{-1}\left(\frac{P_{EW}}{P_{NS}}\right) + 360^\circ \quad IF \quad P_{EW} < 0, \; P_{NS} > 0$$

$$= TAN^{-1}\left(\frac{P_{EW}}{P_{NS}}\right) + 180^\circ \quad IF \quad P_{EW} < 0, \; P_{NS} > 0$$

The development of lateral loads from the FSTF data is illustrated schematically in Figure 4-10. During each test time, strain data from the pair of bending bridges are recorded (Figure 4-10 (a)). Using the relationship in Equation 4.1, orthogonal lateral load time histories at the downcomer end

can be computed and vectorially combined for each time point (Figure 4-10 (b)) to obtain the time traces of resultant load and angle of application (Figure 4-10 (c)).

For air clearing and condensation oscillation, the peak design load is defined as the maximum RSEL observed in the FSTF DBA and IBA tests. For chugging, however, a 95th percentile load derived from the critical chug-related RSEL trace is the defined design load. This 95th percentile load definition is justified based upon the random nature of the chugging phenomenon.

4.3 FATIGUE LOAD CALCULATION

For fatigue evaluation, the number of load reversals in the RSEL trace at different load levels are counted and histograms of the number of reversed cycles versus load level are obtained. Since the direction of load (RSEL) can be arbitrarily oriented at any instant of time, 8 equal and diametrically opposed sectors of 22 1/2° are defined, and individual load histograms are developed for each sector. For the structural evaluation of a downcomer of the FSTF configuration, the peak design lateral load can be used directly as a static equivalent load to analytically determine stresses at any desired location in the critical region near the downcomer vent header intersection. Since the load is based on the maximum peak observed in the RSEL trace, the extreme dynamic response is represented by the static load.

For fatigue evaluation, the stress at a selected critical location of the downcomer/vent header intersection, due to unit lateral static load applied at any desired angle θ, can be determined by analysis, and then used to convert the load reversal histogram to a stress reversal histogram for the selected location. The stress reversal histogram can then be used in conjunction with an appropriate fatigue damage law to evaluate cumulative damage.

Several methods for estimating fatigue damage under random cycling are available in the literature. Some methods make use of the statistical character of the

cycle pattern, as characterized by mean and standard deviation of the signal. Others involve essentially a direct cycle counting approach in which the fatigue damage contribution of each individual cycle is calculated and summed to estimate total fatigue damage. Because some cycling does not adhere to any consistent statistical distribution such as normal or Gaussian, it was decided to use a direct cycle counting approach to evaluate fatigue damage. The Ordered Overall Range (OOR) approach of References 3 and 4 was selected to perform the cycle counting operation.

OOR is an abbreviated cycle counting approach which permits selection of a small number of load reversals which account for a large fraction of the fatigue damage. Figure 4-11 illustrates application of the approach to a simplified load trace. The first step is to select the largest overall range of a load trace from the highest peak to the lowest valley (Points F and U in Figure 4-11(b)). Next, a screening level of some percentage of the largest overall range (50% in Figure 4-11(c)) is selected and all reversals are counted which exceed that screening level, keeping track of the sequence in which the reversals occur. Only reversals which occur in a peak-valley-peak-valley sequence are considered. (Note that in Figure 4-11(d) the range between reversals H and M is actually larger than the counted range between M and R, but the former range was not counted because it was not in the correct sequence and would yield a peak-peak-valley-valley sequence in conjunction with the largest overall range.) The screening level is then reduced incrementally to zero, and a load spectrum of screening amplitude versus number (or percent) of cycles greater than the screening amplitude is produced as illustrated in Figure 4-11(e). The finer the screening level increments the more accurate will be the representation of the actual cycling. The resulting OOR load spectrum can be used to estimate fatigue damage in conjunction with any fatigue curve and cumulative damage law desired. In many cases, only the upper portion of the load spectrum is required to obtain a reasonably accurate damage estimate since higher stress cycles tend to dominate fatigue damage calculations. For the fatigue load definition, only RSEL reversals which are greater than a threshold of 5% of the maximum load range were counted for the histograms, since cycles of smaller magnitude do not contribute to significant fatigue usage.

Using the OOR method, a computer program was developed to accurately perform the cycle counting and to generate load reversal histograms. Such histograms have been generated for both the DBA and IBA condensation oscillation and chugging load definitions. Air clearing is not considered to be of sufficient duration to contribute to fatigue damage and thus no histograms were generated for this load. The histograms are generated for each of 8 downcomer sectors as shown in Figure 4-12. A sample histogram is shown in Figure 4-13. These RSEL reversal histograms are converted into stress reversal histograms and then used for fatigue evaluation. This conversion technique is explained in Section 4.5.

4.4 CHUGGING SYNCHRONIZATION LOAD CALCULATION

For the case of pool chug synchronization, the probability of exceeding a given force magnitude at least once during multi-downcomer chugging is determined from probability of exceedance curves derived from the FSTF data shown in Figure 4-14. The load per FSTF downcomer can be obtained from the curves for various numbers of downcomers once an acceptable probability level of exceedance has been established. A probability of exceedance of 10^{-2} is conservative for this application. The resultant load in any direction due to pool chug synchronization may now be determined by multiplying the number of downcomers being considered by the load per downcomer. It is necessary to scale this resultant FSTF load by the same scale factor used previously for scaling the 95th percentile FSTF chugging load to determine the resultant lateral load on a plant-unique Mark I vent system.

4.5 APPLICATION TO MARK I DOWNCOMERS

The downcomer lateral loads defined for the FSTF consist of peak design loads and histograms of load reversals. As discussed in the previous sections, both of these representations of the loading have been developed as equivalent static representations of dynamic response. In order to scale these equivalent static quantities from the FSTF to obtain equivalent static quantities for a specific plant, it is obvious that the scaling will depend on the dynamic properties of the two systems. A simple scaling procedure based on the natural frequency of the downcomer and the predominant frequency of the lateral load

has been devised. For the peak design load, the application methodology described herein is essentially a scaling procedure based on the ratio of the dynamic load factors (DLF's) between the parent system (FSTF) and the system for which the downcomer lateral load is sought.

In Reference 5, DLF is defined as the ratio of the maximum dynamic deflection to the deflection which would have resulted from the static application of the load. For time varying loads, DLF is usually taken as the maximum value during the period of interest. This factor is typically a function of: (1) The driving frequency (or duration) of the disturbing force, Ω; (2) the natural frequency of free vibration of the system, ω; (3) the structural damping, β; and (4) the shape of the disturbing force. For example, when the load is sinusoidal, as representative of the condensation oscillation phenomenon, the expression for the DLF is:

$$DLF = \frac{1}{\sqrt{\left(1 - \frac{\Omega^2}{\omega 2}\right)^2 + 4\left(\frac{\beta\Omega}{\omega 2}\right)^2}}$$

where the condensation oscillation driving frequency Ω was observed from the FSTF tests to be approximately 5.5 cps.

This relationship is shown in Figure 4-15 for various values of β/ω, which is a measure of system damping. From Figure 4-15 it is obvious that for constant Ω, the higher the ω, implying a stiffer system, the smaller the DLF for Ω/ω ratios less than unity.

For the chugging phenomenon, the load is approximated as a symmetrical triangular pulse. From Reference 5, the dynamic load factor for this forcing function is defined as:

$$DLF = \frac{2}{\omega t_d}\left[2\sin\omega(t - t_d/2) - \sin\omega t - \sin\omega(t - t_d)\right]$$

where the duration of the chug load t_d was observed from the FSTF tests to be approximately 0.005 seconds.

The time-dependency of this equation can be removed by approximating the time to maximum response to be T/4, where T is the natural period of the downcomer. This is a valid assumption since chugging loads are of short duration and thus the downcomer would oscillate freely after receiving an impulsive load. The time to maximum response would then be one-quarter of the fundamental period of the structure. Using this approximation, the above equation becomes:

$$DLF = \frac{2}{\omega t_d}\left[2\cos\left(\frac{\omega t_d}{2}\right) - \cos(\omega t_d) - 1\right]$$

These dynamic load factors for condensation oscillation and chugging form the basis for the application methodology. The FSTF loads are scaled to individual plant loads according to the following relationship:

$$P_{MAX} = P_1 \times \left(\frac{DLF}{DLF_1}\right) \qquad (4.2)$$

where P_1 = downcomer lateral load for the parent system (FSTF)

P_{MAX} = downcomer lateral load for the system of interest

DLF = DLF for the system of interest

DLF_1 = DLF for the parent system (FSTF)

For the fatigue histograms, the maximum RSEL reversal levels are scaled in a manner similar to the scaling of the peak design load, i.e., based on DLF's. The number of cycles of load reversal are also scaled by the ratio of the actual condensation oscillation or chugging durations specified for the plants to those respective durations observed during the FSTF tests.

The dynamic load factors depend upon the natural frequencies of the single-degree-of-freedom systems representing the downcomer/vent header structures. For the range of the Mark I plant downcomer geometries, the ratio of the dynamic load factors between the FSTF and a plant-unique downcomer is essentially independent of the direction of load application. This was verified by calculating and comparing the DLF ratios for the FSTF and a representative Mark I plant in the North-South and East-West directions. These directions were selected because their associated frequencies bound all possible downcomer frequencies. The resulting DLF ratios in the two directions agreed to within 0.5 percent. Therefore, for consistency in using this in this procedure the dynamic load factors used in the scaling relationship are to be determined on the basis of the downcomer frequencies in the East-West direction.

The natural frequency in the East-West direction can be determined once the rotational stiffness of the downcomer/vent header junction and the mass moment of inertia of the downcomer in this principal direction have been ascertained. The mass moment of inertia must include the added mass of the water for the submerged portion of the downcomer.

For condensation oscillation, the maximum FSTF DBA loads were observed from the data to occur within ±22 1/2° of the East-West direction, i.e. in the plane of the downcomer pairs, as identified by sectors 4 and 5 in Figure 4-13. Similarly, maximum IBA loads were observed to occur within ±45° of the East-West direction, i.e., sectors 3 through 6 in Figure 4-13. Therefore, the plant-unique design load P_{max} determined from Equation 4.2 for either a DBA or IBA evaluation must be applied to the end of the plant-unique downcomers within the above-defined respective directions such as to maximize the stresses at the downcomer/vent header junction.

The direction of the maximum chugging loads was observed from the FSTF tests to be random. The maximum design chugging load must therefore be applied to the end of the plant-unique downcomers in a direction which maximizes the stresses at the downcomer/vent header junction.

This DLF scaling approach was verified by comparing the finite element predicted dynamic response of the FSTF and Cooper Station downcomers with the corresponding response predicted by the DLF scaling procedure.

As an example, the Cooper Station and FSTF downcomer/vent systems were analyzed using the finite element method, and the results compared with those obtained from a DLF scaling approach. The finite element model used to represent the FSTF downcomer/vent header system is depicted in Figure 4-2, and the structural and material properties are given in Table 4-2. The Cooper Station downcomer/vent header system was similarly modeled using the properties given in Table 4-2.

The rotational stiffness ($k_{rC.S.}$) of the Cooper Station downcomer/vent header junction was obtained by scaling the FSTF downcomer/vent header stiffness using the following empirical relationship (Reference 6):

$$k_r \propto \frac{\pi E d^2 t}{8} \left[\left(\frac{T}{D} \right)^{3/2} \left(\frac{T}{t} \right) \left(\frac{D}{d} \right) \right]$$

where

d = mean diameter of downcomer

D = mean diameter of vent header

t = wall thickness of downcomer

T = wall thickness of vent header

E = elastic modulus

and $\propto$ indicates "directly proportional".

Using dimensions for the Cooper Station and FSTF downcomer/vent header structures as given in Table 4-2, the rotational stiffness of the Cooper Station downcomer/vent header junction was found to be:

$$(k_r)_{C.S.} = \sqrt{\frac{D_{FSTF}}{D_{C.S.}}} \times (k_r)_{FSTF}$$

It is desired to scale the experimentally determined blowdown response of the FSTF downcomer/vent header structure to other Mark I downcomer/vent header structural configurations. The scaling law, using the single degree of freedom assumption, is given as

$$M = M_1 \left(\frac{DLF}{DLF_1}\right)\left(\frac{L}{L_1}\right) \qquad (4.3)$$

where

M = moment in downcomer of a particular Mark I plant at a moment arm length L from the downcomer tip,

M_1 = moment at the bending bridge in the FSTF downcomer at a moment arm length L_1 from the downcomer tip,

DLF = dynamic load factor for a particular downcomer/vent header system,

DLF_1 = dynamic load factor for the FSTF downcomer/header system.

It is seen from Equation 4.3 that the moment in a Mark I downcomer which is geometrically similar to the FSTF downcomer is simply proportional to the moment in the FSTF downcomer, the ratios of the moment arm lengths and the DLF's. As previously discussed, the DLF's are defined differently for the condensation oscillation and chugging regions of a blowdown.

A finite element analysis of the FSTF downcomer and the Cooper Station downcomer was performed for both condensation oscillation and chugging loads. The moment response of the FSTF downcomer number 6 subjected to simulated chugging and condensation oscillation loadings is shown in Figures 4-16 and 4-17, respectively. The DLF scaling procedure was verified by applying Equation 4.3 to the maximum moments indicated in Figures 4-16 and 4-17. Applying Equation 4.3 for a chug load resulted in a maximum moment in the Cooper Station downcomer of 106 in-kips which compared very well with 105 in-kips obtained from the finite element analysis. For the condensation oscillation load, the maximum moment for the Cooper Station downcomer was 248 in-kips as compared to 284 in-kips obtained in the finite element analysis.

Once the number of cycles of load reversals has been determined and scaled to the individual plant, then the RSEL reversals must be transformed into downcomer/vent header stress reversals. One method which can be used to transform the loads to stresses at a particular point "A" near the downcomer/vent header intersection, Figure 4-18, is through a load-stress transformation matrix. This matrix may be obtained from a detailed static finite element analysis of the downcomer/vent header structure. First, a unit load F_N would be applied at the downcomer end in the North direction (Figure 4-18) to obtain

$$\sigma_a = K_N F_N \tag{4.5}$$

where σ_a is a representative stress measure to be used in fatigue analysis. Similarly, a unit load F_E would be applied at the downcomer end in the East direction to obtain a similar stress measure σ_b as

$$\sigma_b = K_E F_E \tag{4.6}$$

which upon combining stresses yields

$$\sigma = \sigma_a + \sigma_b = (K_N \; K_E) \begin{bmatrix} F_N \\ F_E \end{bmatrix} \tag{4.7}$$

3620038

For an arbitrary loading $\underline{P}$ having components P_N and P_E, the resultant stress is

$$\sigma = \underline{K}\,\underline{P} \qquad (4.8)$$

where the transformation matrix $\underline{K}$ will, in general, be different for different locations of stress determination.

The total number of stress reversals at a location selected for fatigue evaluation is obtained by summing the stress reversals produced at the location by the condensation oscillation or chugging RSEL reversals in each sector.

4.6 CONSIDERATIONS FOR BRACED DOWNCOMERS

The preceding methodology for determination of downcomer lateral loads was originally developed for unconstrained downcomer systems based upon experimental data obtained from the FSTF. Subsequent to the initiation of testing in the FSTF, a decision was made by several of the Mark I plants to brace their downcomer/vent header systems. Because of this trend toward stiffening the downcomers, additional work is in progress to use the existing FSTF data base to develop DBA and TBA condensation oscillation and chugging loads for tied downcomers.

Table 4-1

COMPARISON OF DOWNCOMER & DOWNCOMER/VENT HEADER JUNCTION STIFFNESSES

Plant	Downcomer Type	Header Internal dia. Di(ft)	Header Wall Thick-ness T(in.)	Down-comer Internal dia. di(in.)	Down-comer Wall Thickness (junction) t(in.)	Distance Header & to down-comer edge H(ft)	Down-comer Length (approx) h(ft)	Down-comer Stiffness K_d (lb/in)	Junction Stiffness K_j (lf/in)	Ratio k_d/K_j
Monticello	II	4.75	0.25	23.5	0.375	11.0	9.314	84800	1280	66.5
Millstone		4.75		24.0	0.5	10.354	8.668	112000	1500	74.5
Dresden 2,3		4.833		24.0	0.5	10.125	8.409	123000	1580	77.4
Quad Cities 1,2		4.833		24.125	0.375	10.125	8.409	125000	1590	78.2
Vermont Yankee		4.75		23.5		11.0	9.314	84800	1280	66.5
Pilgrim		4.75		24.0		10.354	8.668	112000	1500	74.5
Peach Bottom 2,3		4.833		23.625		9.0	7.284	180000	2080	86.6
Fitzpatrick		4.75		23.5		10.667	8.981	94600	1370	68.9
Cooper Station		4.167		23.5		10.125	8.645	106000	1580	67.1
Hatch 1		4.5		23.5		9.875	8.277	121000	1660	72.8
Hatch 2		4.5		23.5		10.208	8.610	107000	1530	70.0
Fermi 2		4.25		23.5		10.125	8.616	107000	1580	68.0
Brunswick 1,2		4.5		24.25		9.417	7.819	157000	1920	82.0
Oyster Creek	I	4.583		23.5	0.5	10.479	8.851	98800	1440	68.7
Nine Mile Pt.	I	4.792	0.313	24.0	0.688	9.0	7.297	188000	3710	50.6
Browns Ferry 1,2,3	IV	4.75	0.5	23.5	0.25	10.875	9.181	88500	7430	11.9
Duane Arnold	III	3.5	0.25	23.5	0.25	9.5	7.74	148000	2150	68.7

Table 4-2

FSTF AND COOPER STATION DOWNCOMER/VENT HEADER PROPERTIES AND NATURAL FREQUENCIES

MATERIAL PROPERTIES	FSTF	COOPER STATION
Elastic Modulus (lb/in^2)	30×10^5	30×10^6
Poisson's Ratio	0.27	0.27
Density: ($slug\text{-}ft/in^4$) Downcomer	7.32×10^{-4}	7.32×10^{-4}
D.C. with Added Mass	2.66×10^{-3}	2.66×10^{-3}
STRUCTURAL PROPERTIES		
L_1 (in)	55.69	60.64
L_2 (in)	45.12	51.30
L_3 (in)	40.0	51.30
A_1 (in^2)	28.127	28.127
A_2 (in^2)	18.653	18.653
I_1 (in^4)	2004.60	2004.60
I_2 (in^4)	1315.34	1315.34
K_r (in-lb/rad)	2.165×10^7	2.313×10^7
NATURAL FREQUENCIES		
ω_1	6.36	6.37
ω_2	219.	173.
ω_3	417.	346.
ω_4	606.	617.

A-cross sectional area

I-area moment of inertia

L_3-submergence depth

K_r-rotational spring stiffness

Table 4-3

COMPARISON OF FSTF AND MARK I CONTAINMENT SIGNIFICANT WETWELL DIMENSIONS

		FSTF	Range of MK I Plants	Duane Arnold
Diameter of wetwell (I.D.) ft		27.66	27.0-31.0	25.66
Diameter of ventline (I.D.) ft		3.90	5.917-6.75	4.75
Diameter of Downcomer (I.D.) ft		1.96	1.9375-2.021	1.958
C of Wetwell to C of Downcomer ft.		4.0	3.0-4.0	0
Distance between downcomers along vent header ft		4.0-5.0	4.0-7.0	5.0
Ventline length ft		35.16	20.302-33.55	27.281
Downcomer length (sum of sections) ft		9.54	6.992-9.917	7.74
Drywell Volume per Downcomer, ft^3		874	1400-2110	2450
Submergence, ft	max	4.5	3.33-5.0	3.395-3.046
	min	1.5	3.0-4.29	
Wetwell operating pressure, psig	max	5.0	$\pm$2.0-$\pm$0.5	$\pm$2.0
	min	0	0.5-0.2	2.0
Wetwell operating temperature °F	max	120	95	82
	min	70	40	80
K factor for vent system		4.8	4.8	-

Table 4-4

COMPARISON OF MAXIMUM RSEL FOR
TIED AND UNTIED FSTF DOWNCOMERS

Test No.	Break Size	Event Type	Downcomer 6 (Untied)	Downcomer 8 (Tied)(a)	Ratio of Tied/ Untied RSEL
M4	IBA	C.O.	1546	1241	0.80
		Chugging	1061	928	0.87
M5	IDA	C.O.	2180	1344	0.62
		Chugging	None	None	
M6	IBA	C.O.	1375	911	0.66
		Chugging	None	None	
M9	IBA	C.O.	1271	1084	0.85
		Chugging	1194	1217	1.02
M8	DBA	C.O.	4122	2517	0.61
		Chugging	None	None	

(a)Tension-only prototypical tie strap

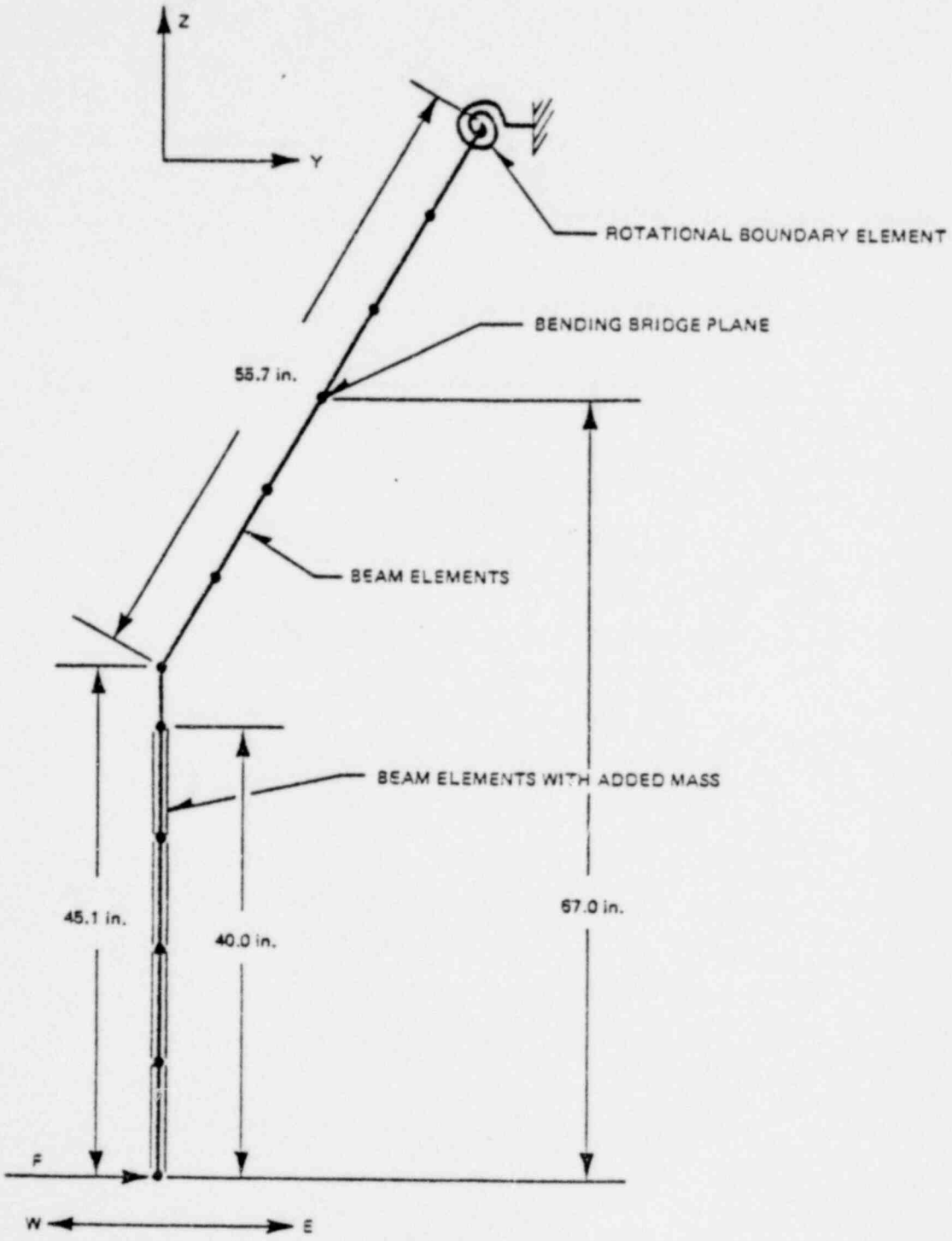

Figure 4-1. Finite Element Model of FSTF Downcomer/Vent Header Structure

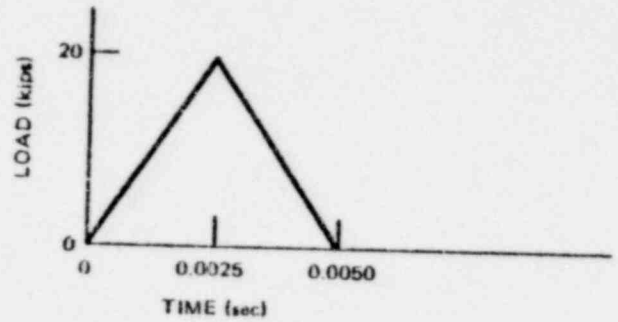

2a. APPLIED "CHUGGING" LOAD

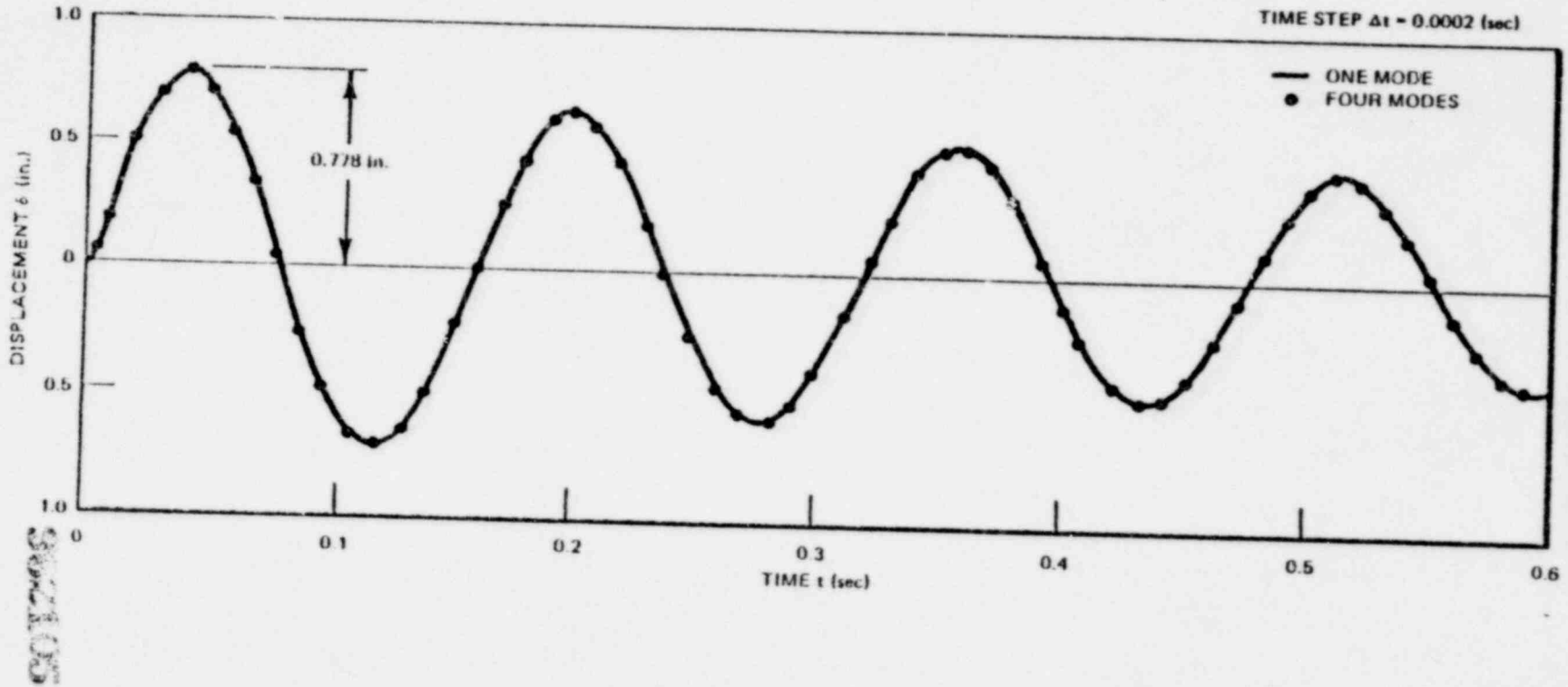

Figure 4-2. Displacement Response of Tip of Downcomer 6 Subjected to a "Chugging" Load

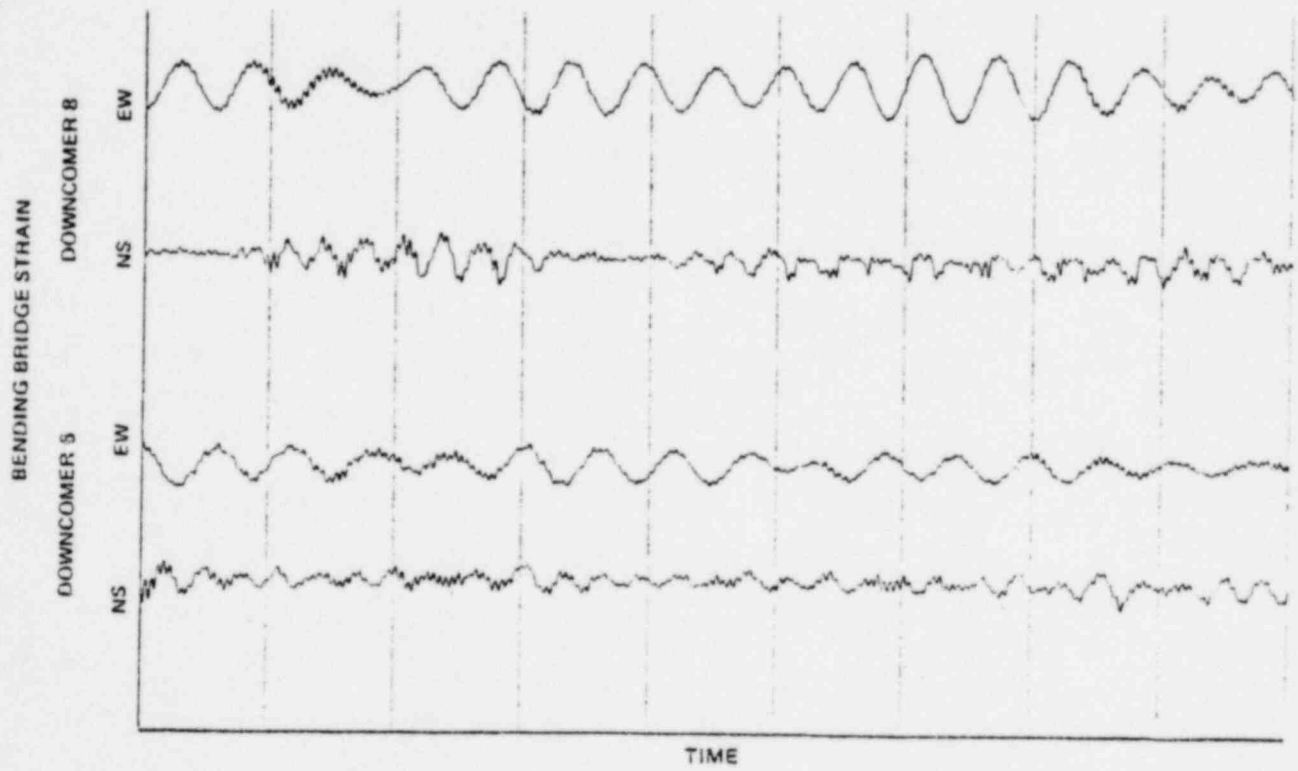

Figure 4-3. Typical Condensation Oscillation Bending Bridge Strain Trace from FSTF Test No. 1

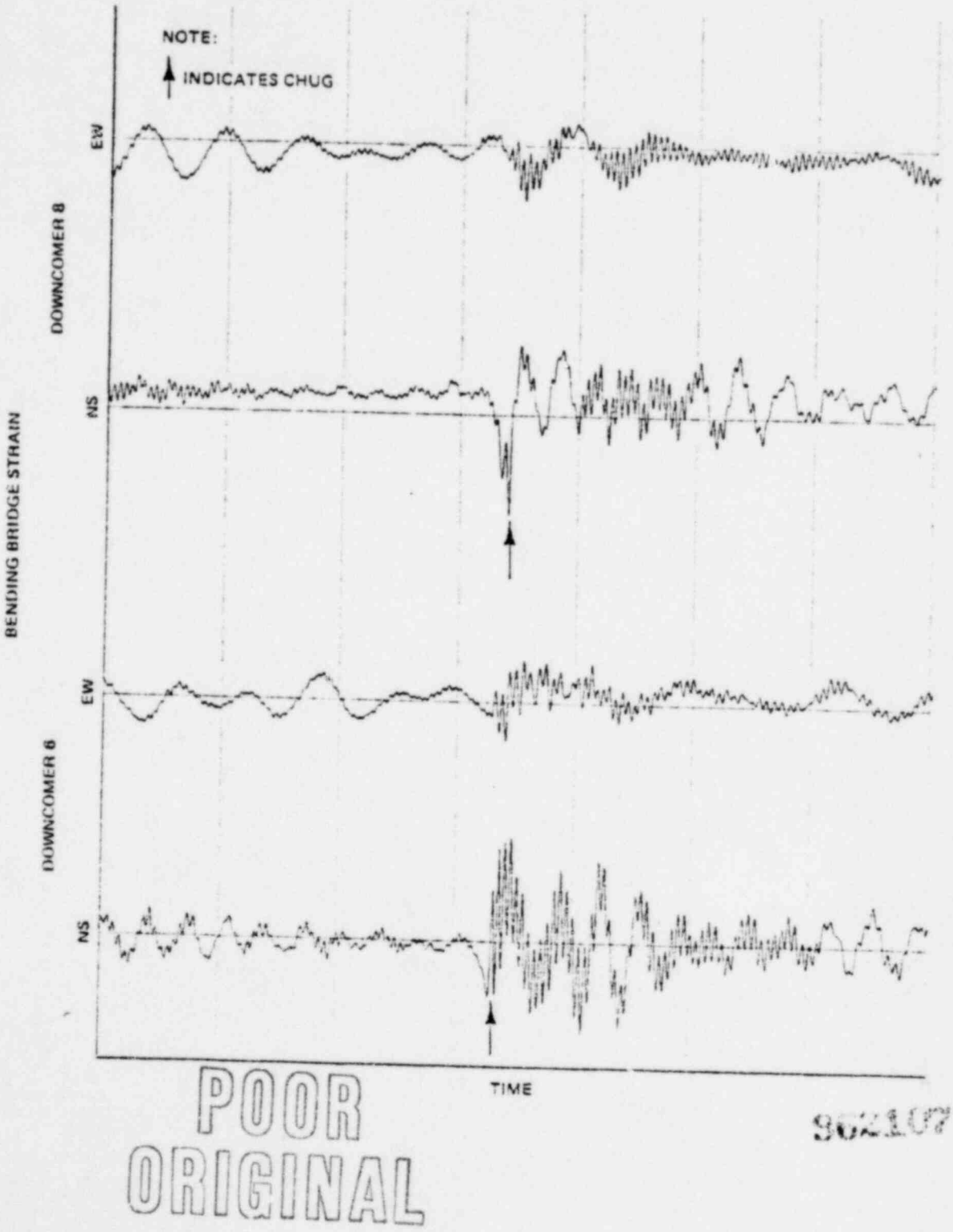

Figure 4-4. Typical Chugging Bending Bridge Strain Trace from FSTF Test No. 1

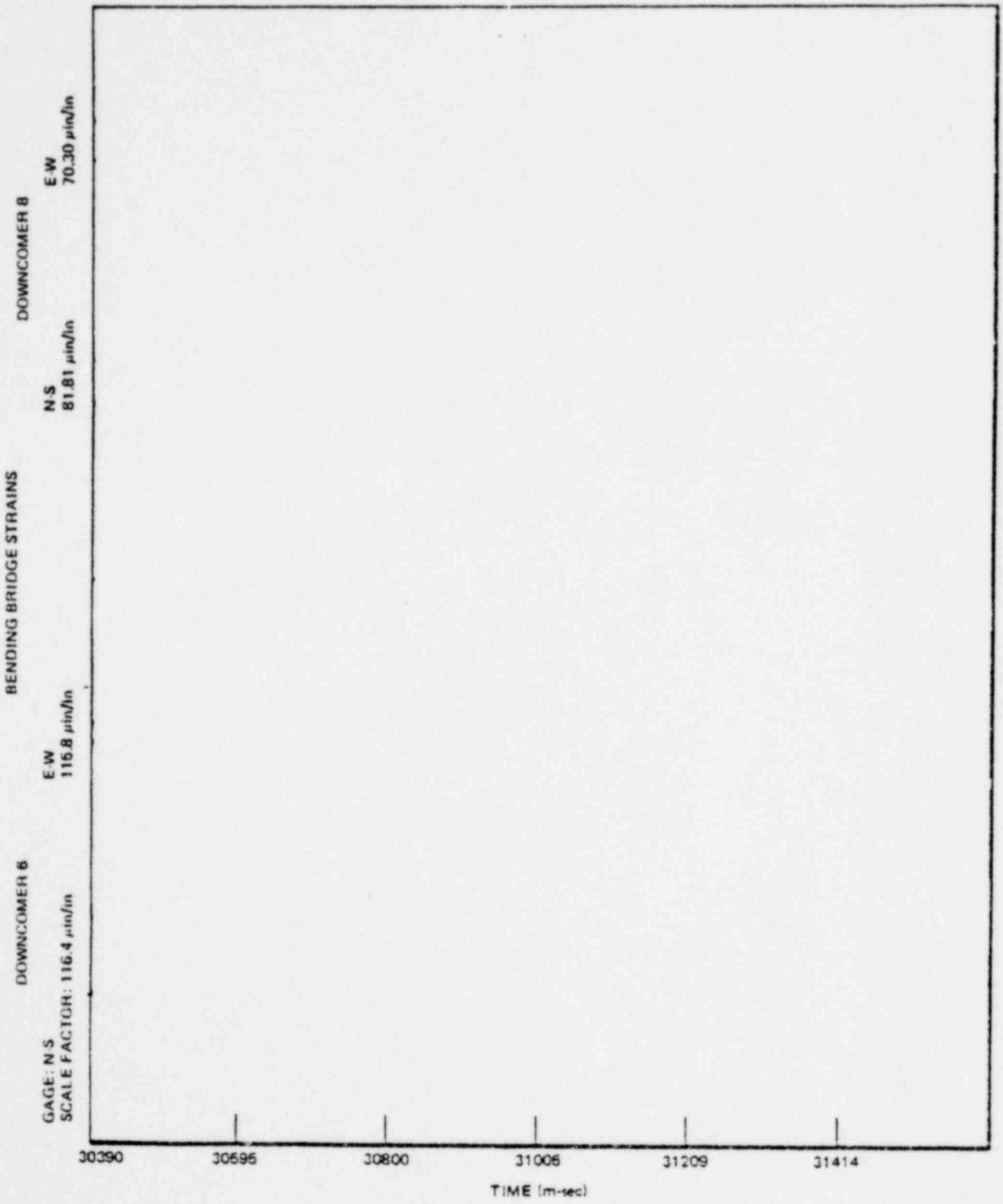

Figure 4-5. Maximum Downcomer Bending Bridge Strain from FSTF Test No. 8

*Proprietary information deleted

962108

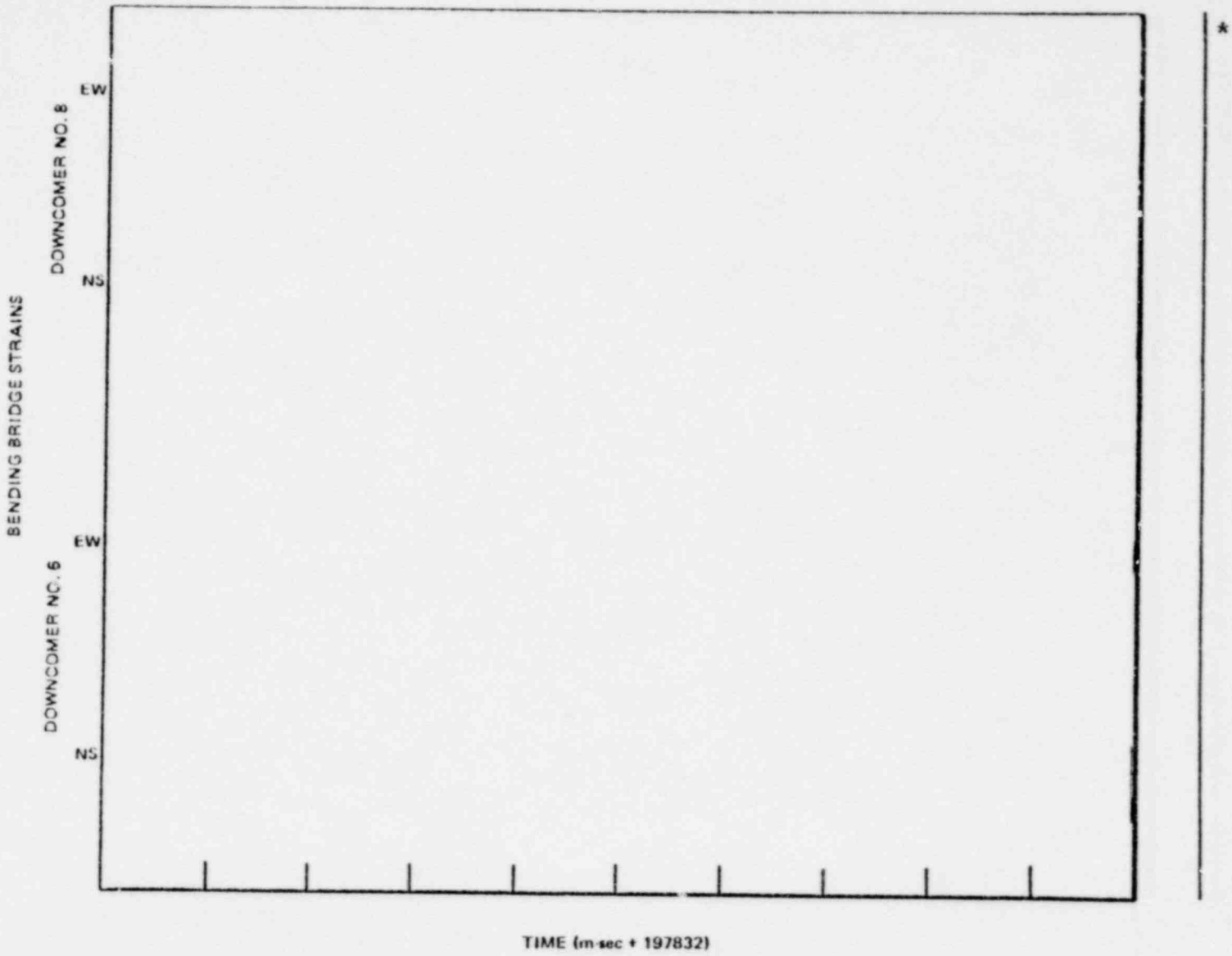

Figure 4-6. Comparison of Bending Response of Downcomer 6 with Chug Times on Downcomer 8

*Proprietary information deleted

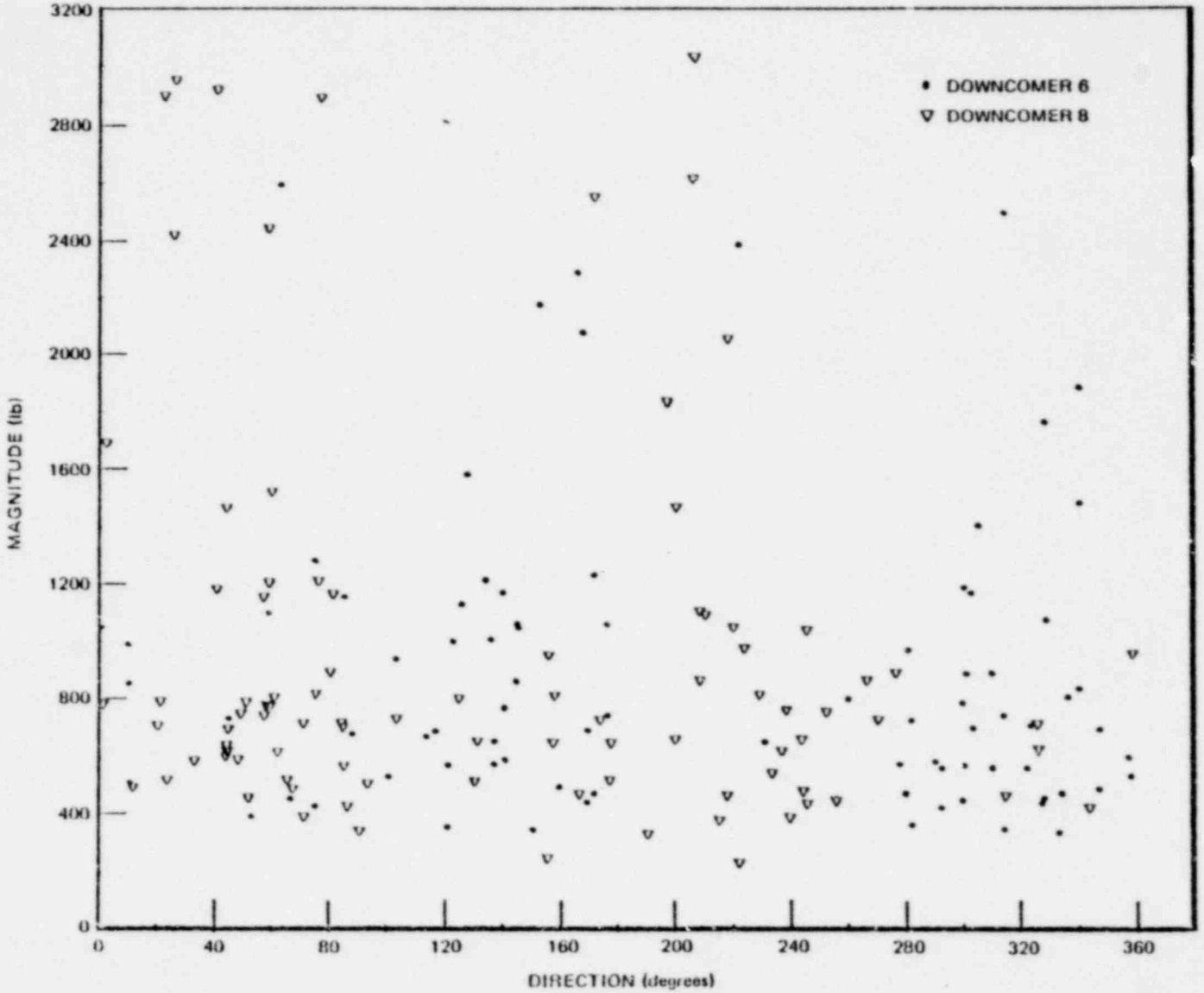

Figure 4-7. Comparison of Peak Chug Directions and Magnitudes from FSTF Test No. 1

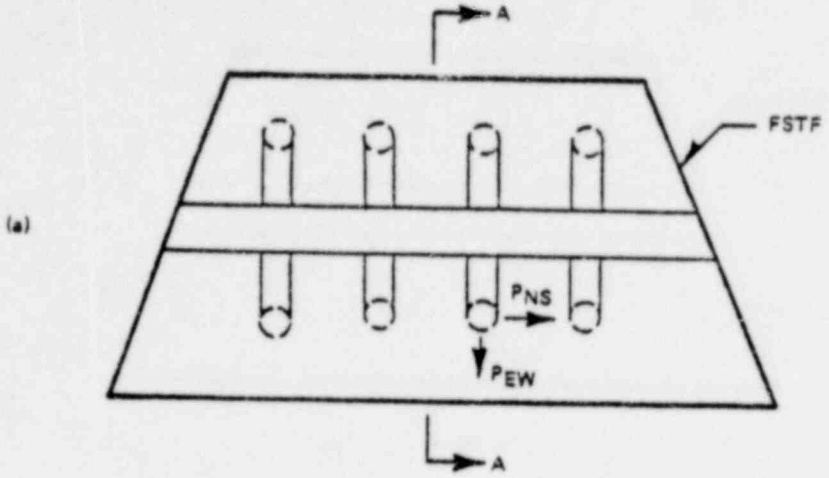

PLAN

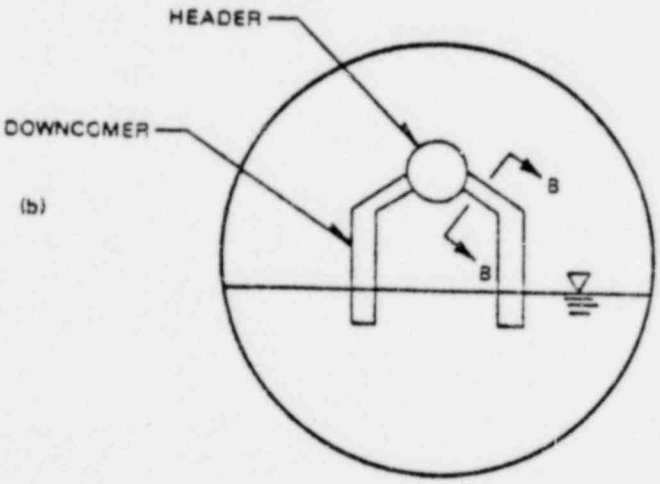

SECTION AA

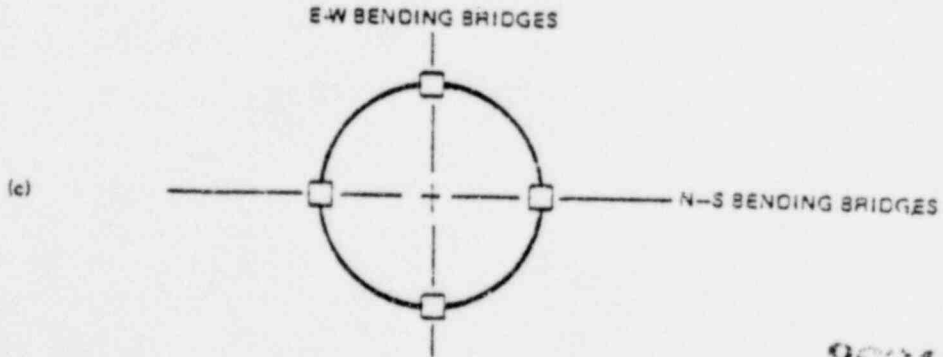

SECTION BB

962111

Figure 4-8. FSTF Downcomer Bending Bridge Locations

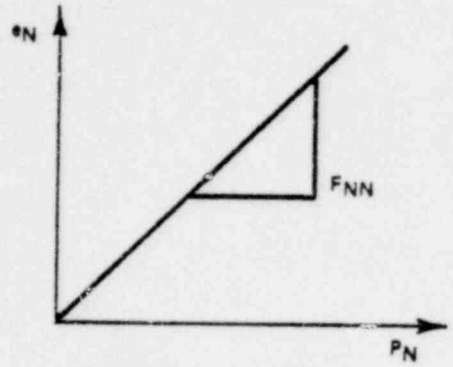

(a) N-S STRAIN FOR N-LOAD

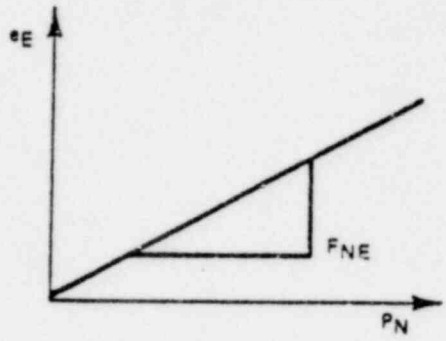

(b) E-W STRAIN FOR N-LOAD

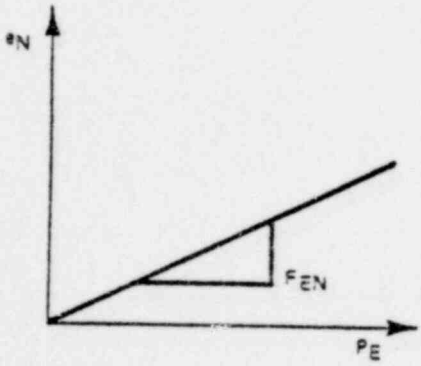

(c) N-S STRAIN FOR E-LOAD

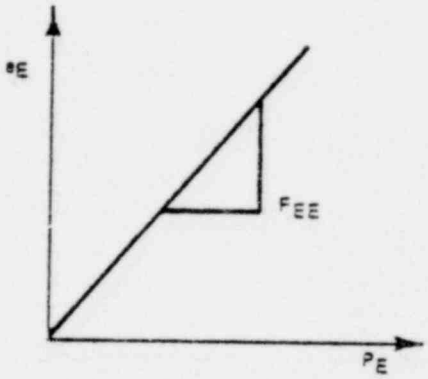

(d) E-W STRAIN FOR E-LOAD

Figure 4-9. Determination of Flexibility Coefficients from Static Calibration Data

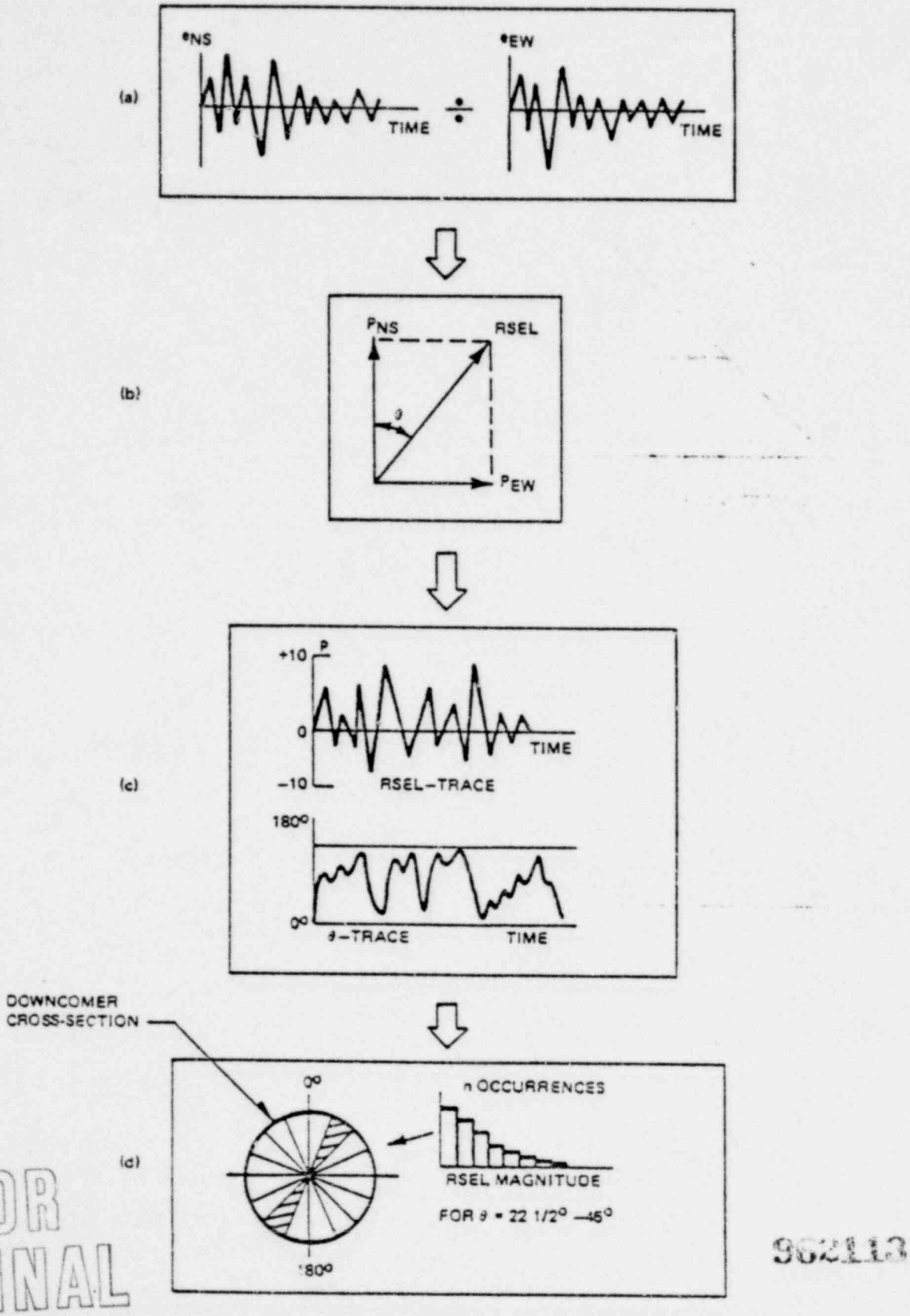

Figure 4-10. Methodology for Determining Downcomer Lateral Loads

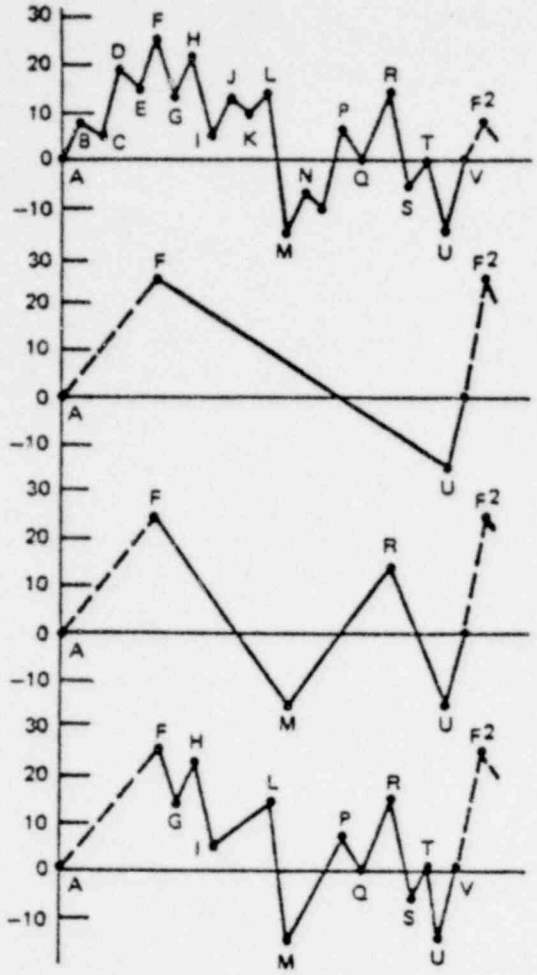

(a) SAMPLE LOAD TRACE CONTAINING 21 RANGES* OF VARYING AMPLITUDE

(b) LARGEST OVERALL RANGE: PEAK TO PEAK AMPLITUDE = 40 ksi

(c) 50% SCREENING LEVEL: 4 RANGES* WITH AMPLITUDE GREATER THAN 20 ksi

(d) 15% SCREENING LEVEL: 12 RANGES* WITH AMPLITUDE GREATER THAN 6 ksi

*(NOTE: NUMBER OF RANGES = NUMBER OF REVERSALS = 2 X NUMBER OF CYCLES)

(e) RESULTING LOAD SPECTRUM:

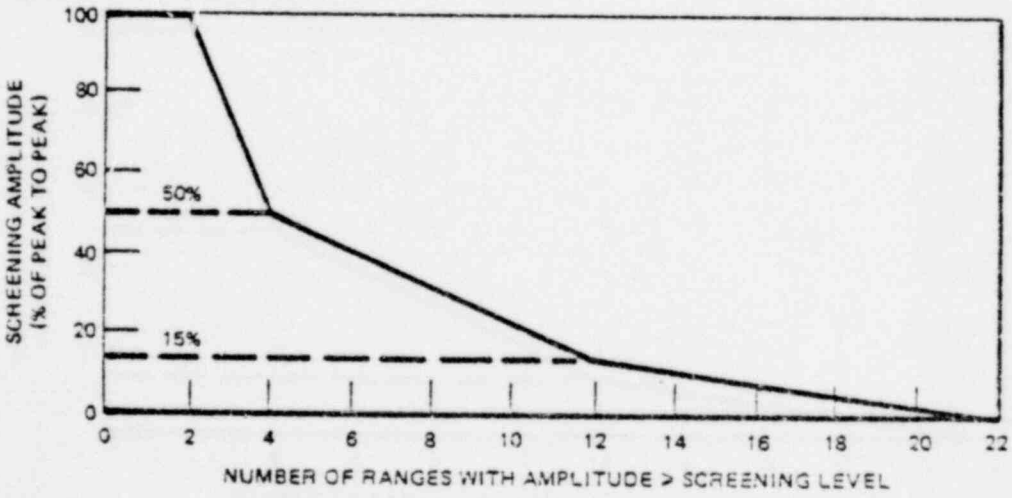

Figure 4-11. Illustration of Ordered Overall Range (OOR) Cycle Counting Approach

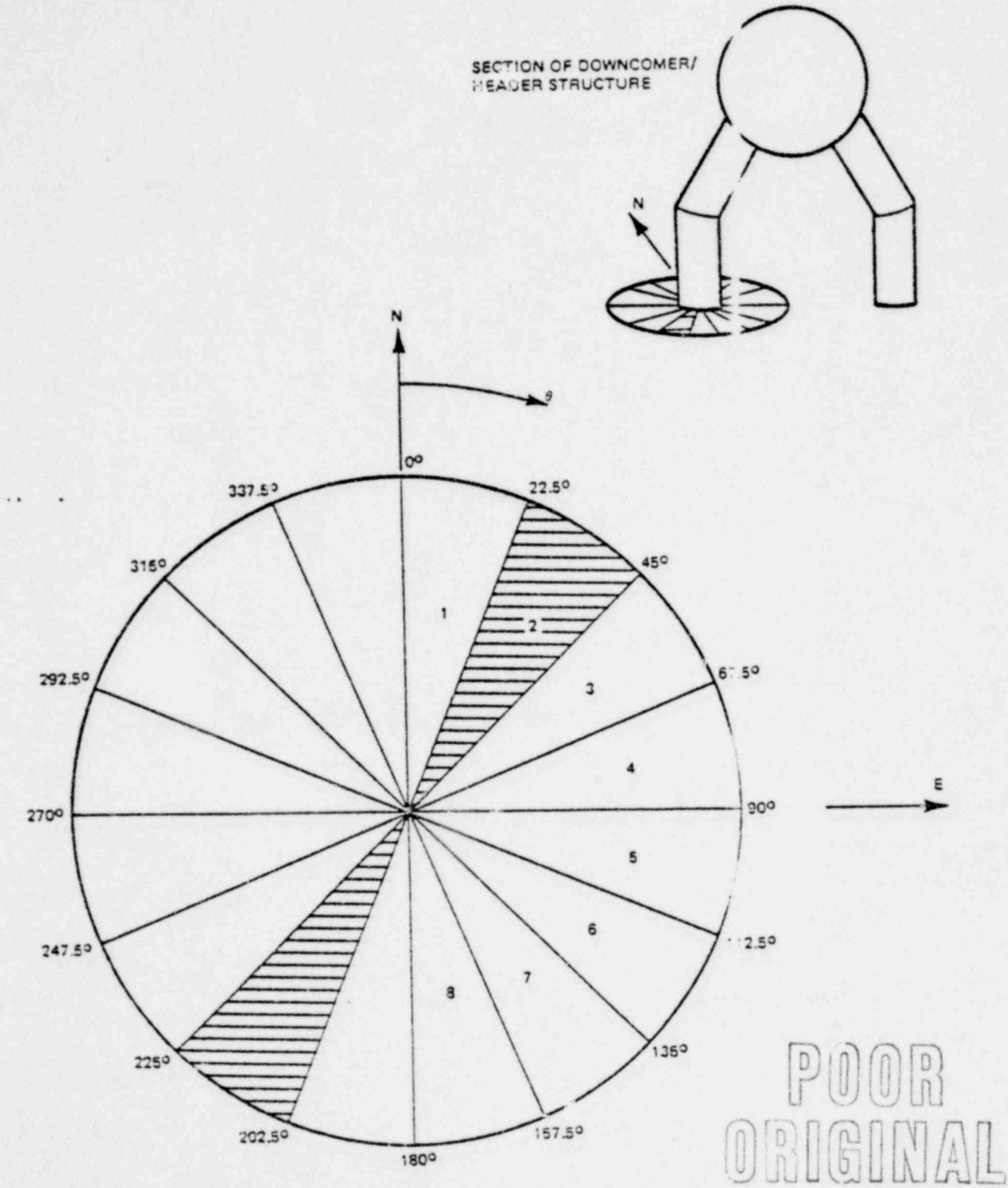

Figure 4-12. Sectors Used to Define Directions of Lateral Loads on Downcomers End

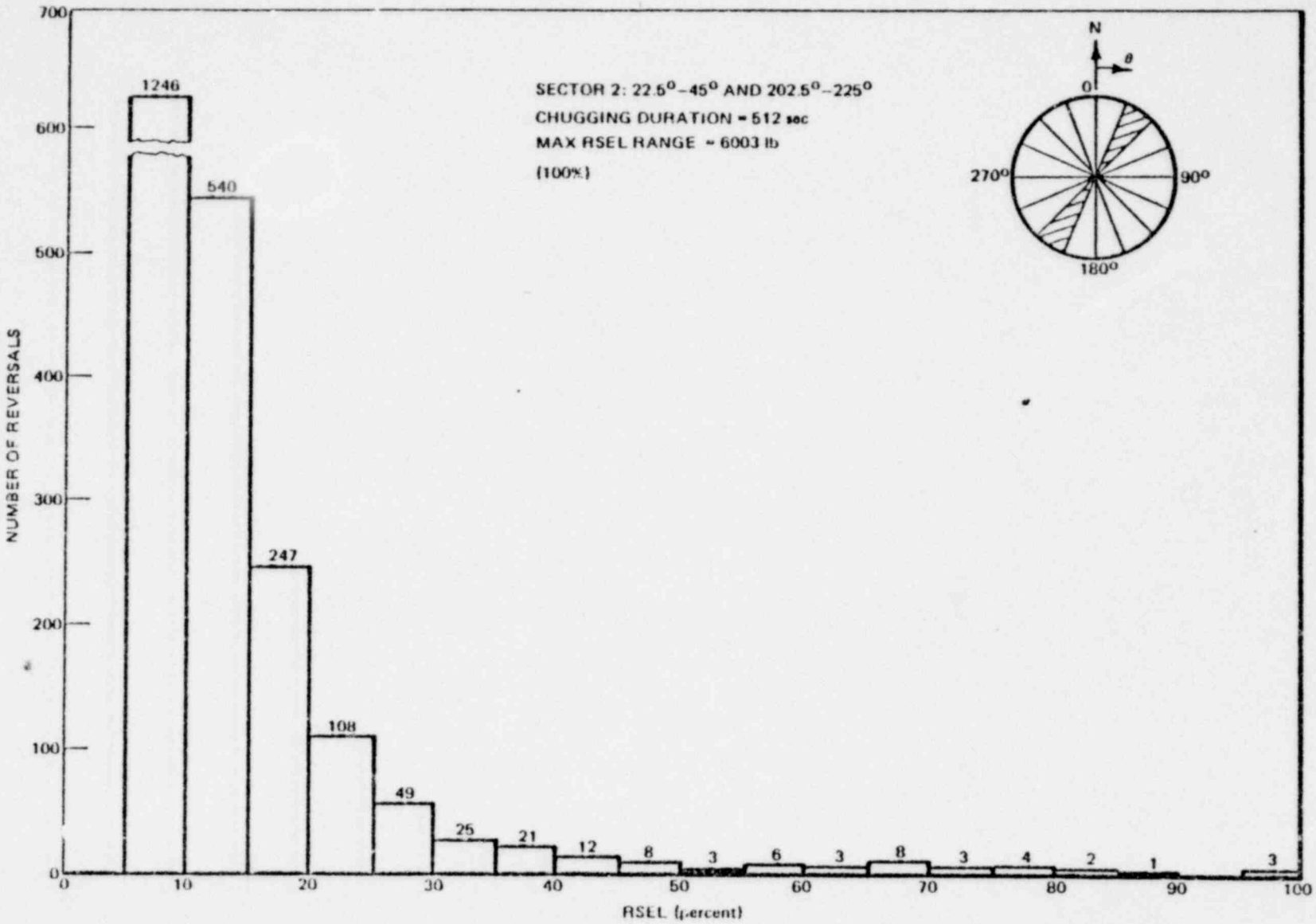

Figure 4-13. Sample Distribution of Chugging RSEL Reversals for a Typical Sector

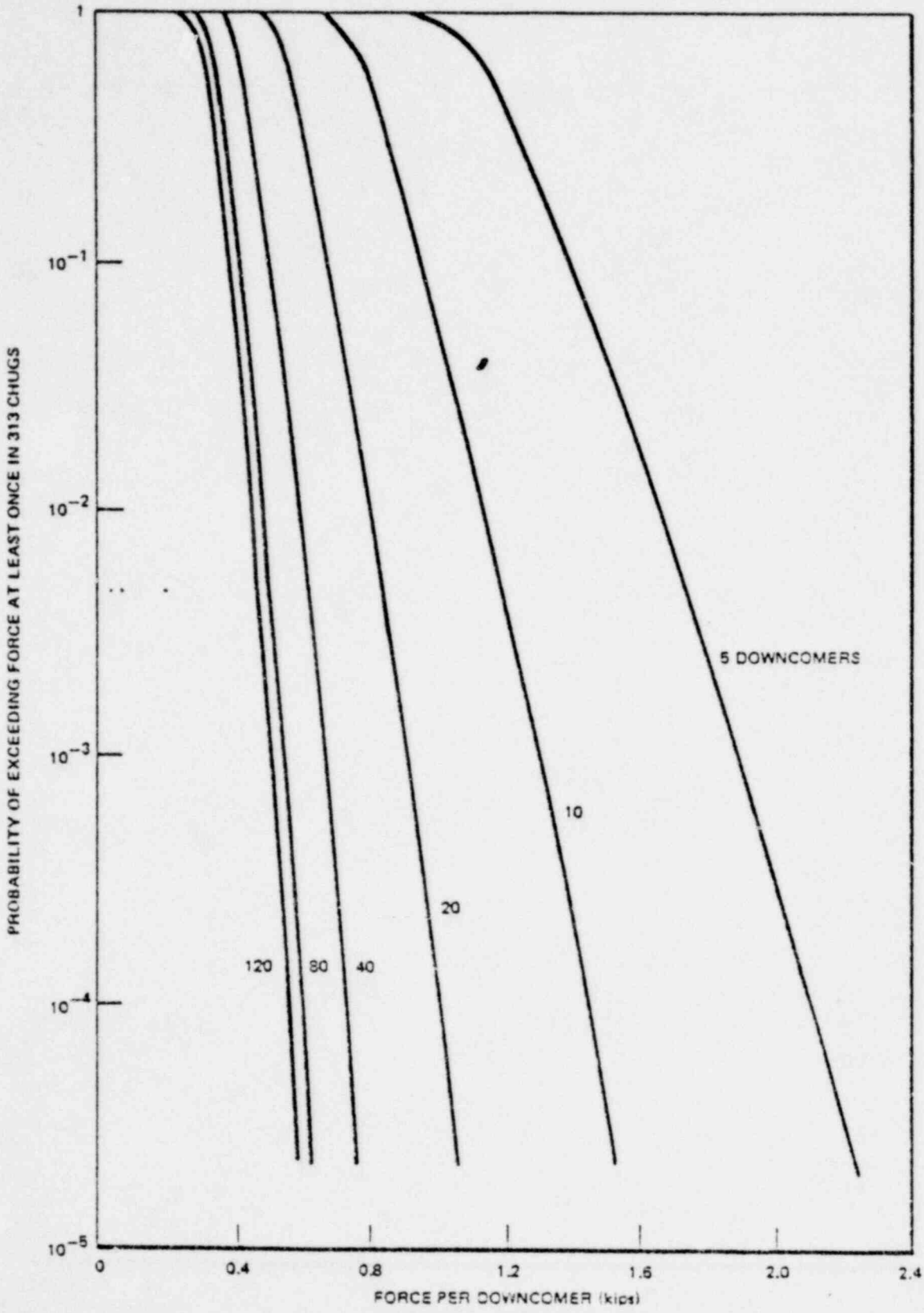

Figure 4-14. Probability of Exceeding a Given Force Per Downcomer For Different Numbers of Downcomers

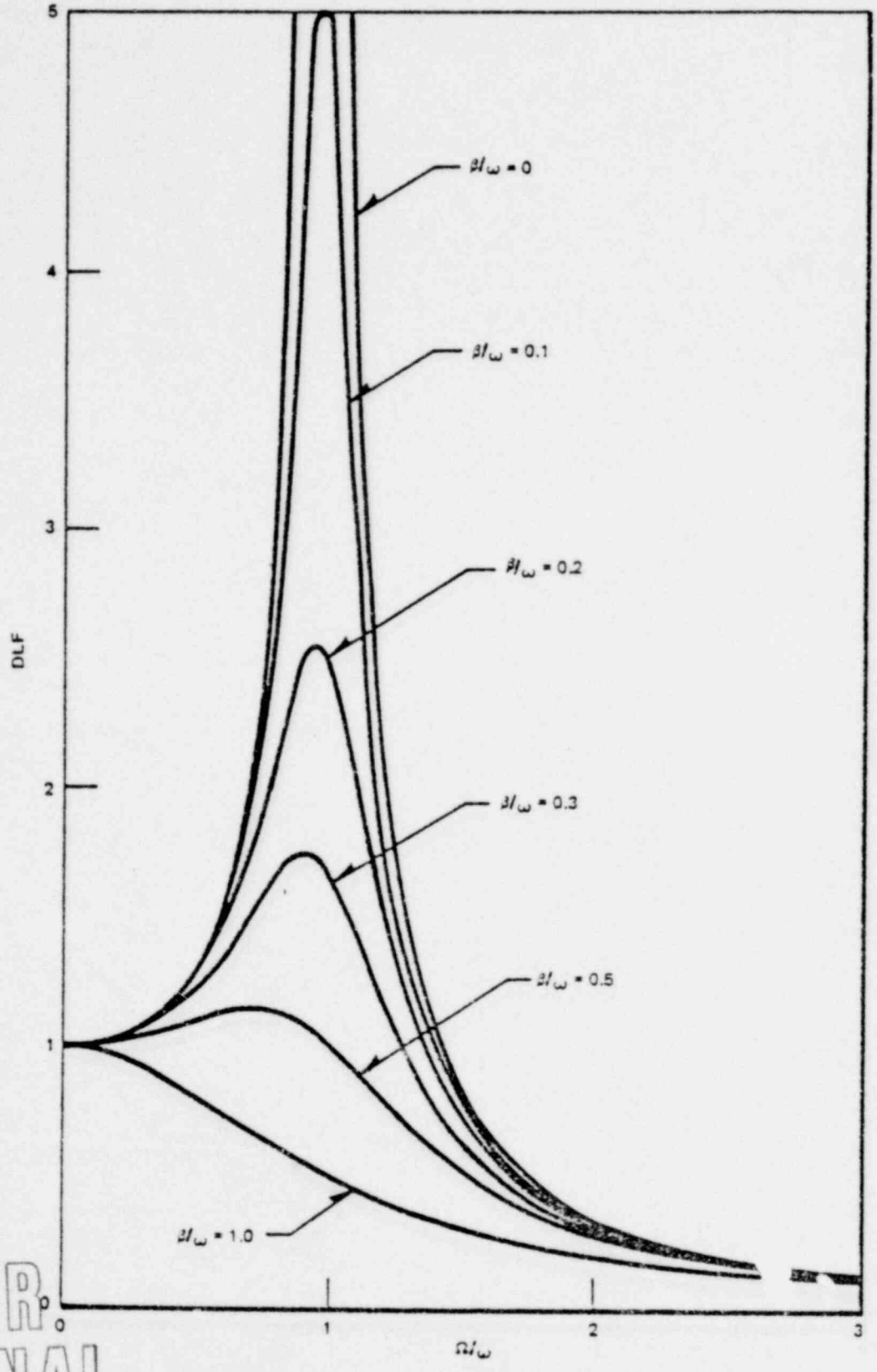

Figure 4-15. DLF's for a Sinusoidal Forcing Function at Different Damping Ratios

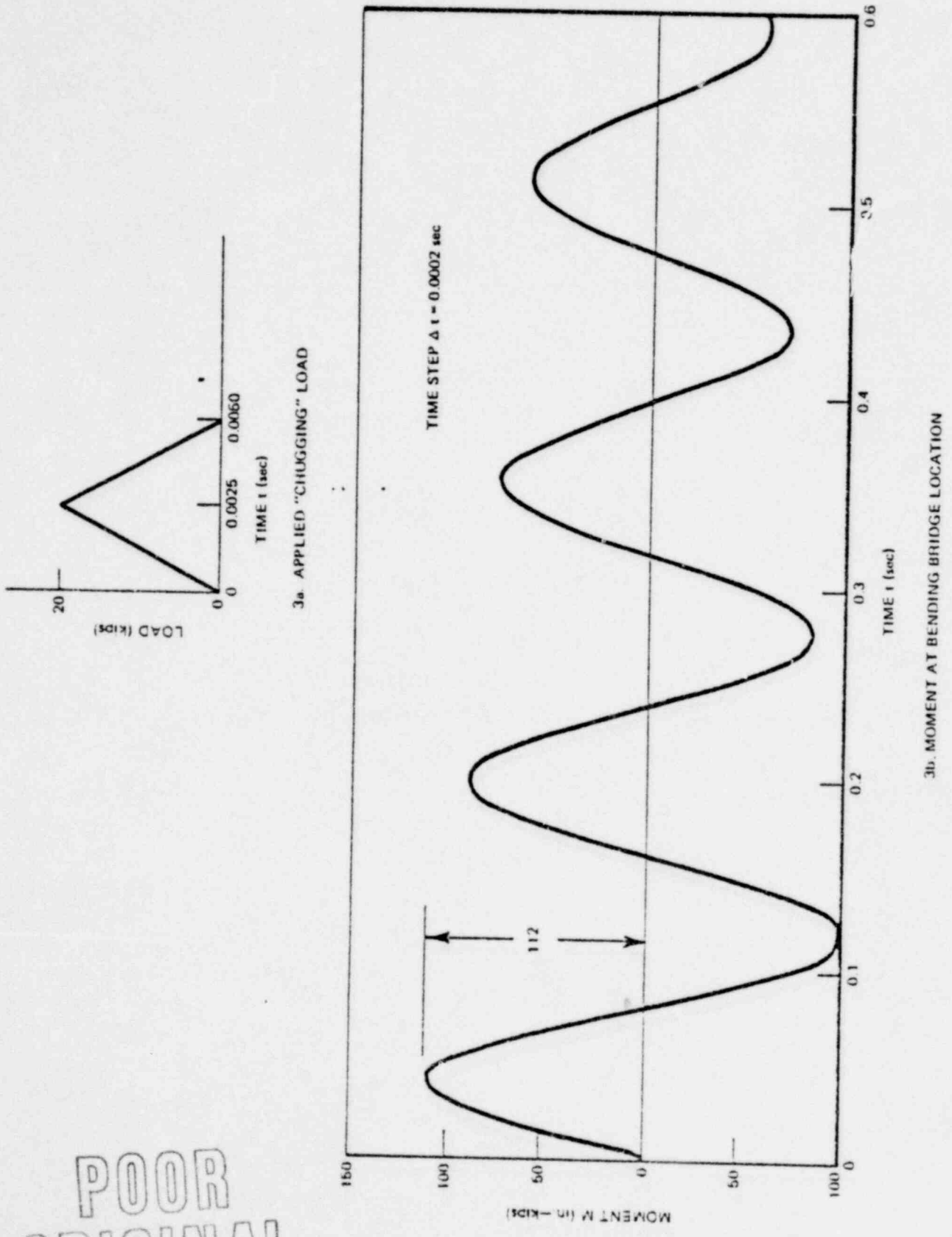

Figure 4-16. Moment Response of FSTF Downcomer 6 Subjected to a "Chugging" Load

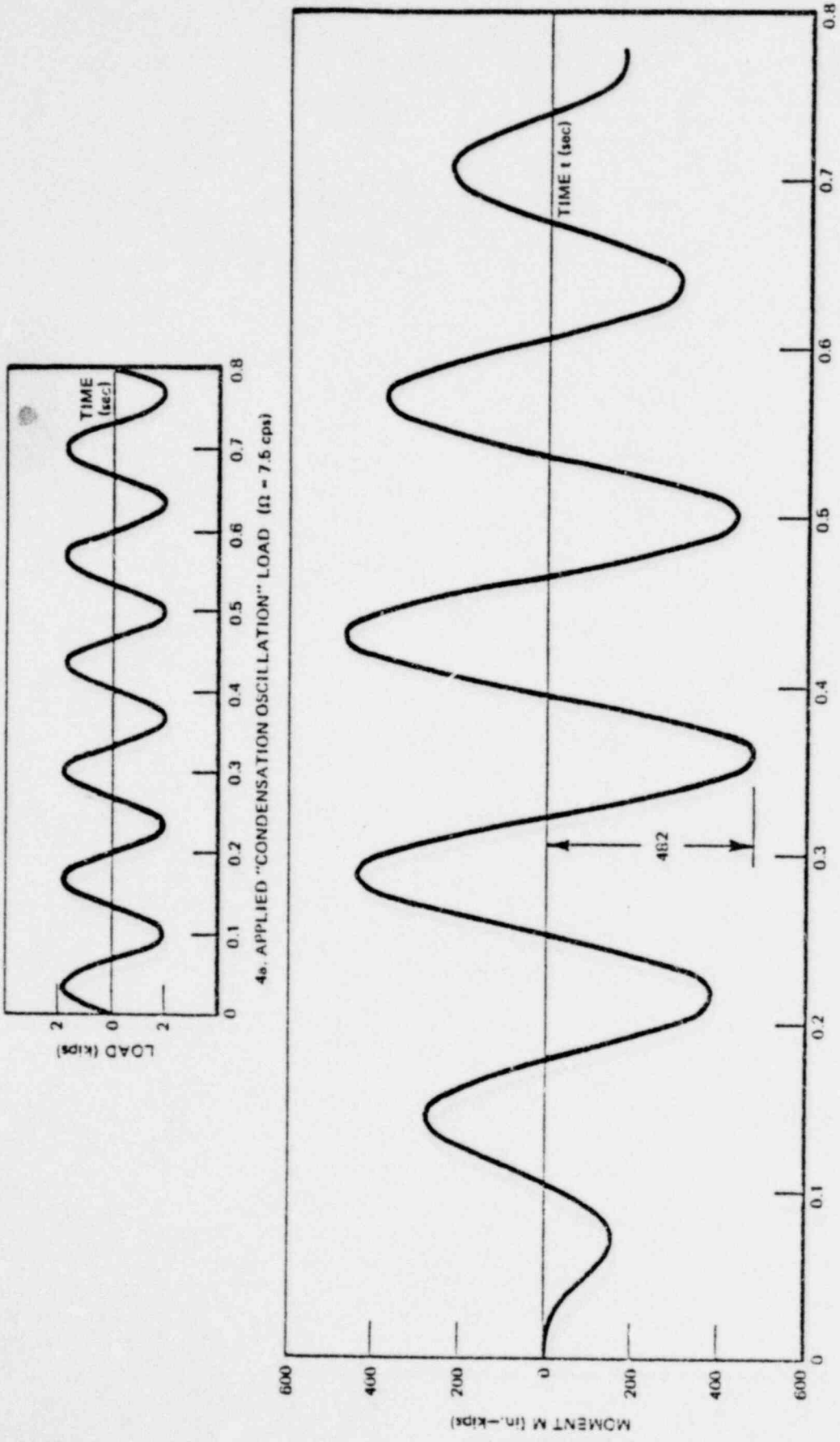

Figure 4-17. Moment Response of FSTF Downcomer 6 Subjected to "Condensation Oscillation" Loading

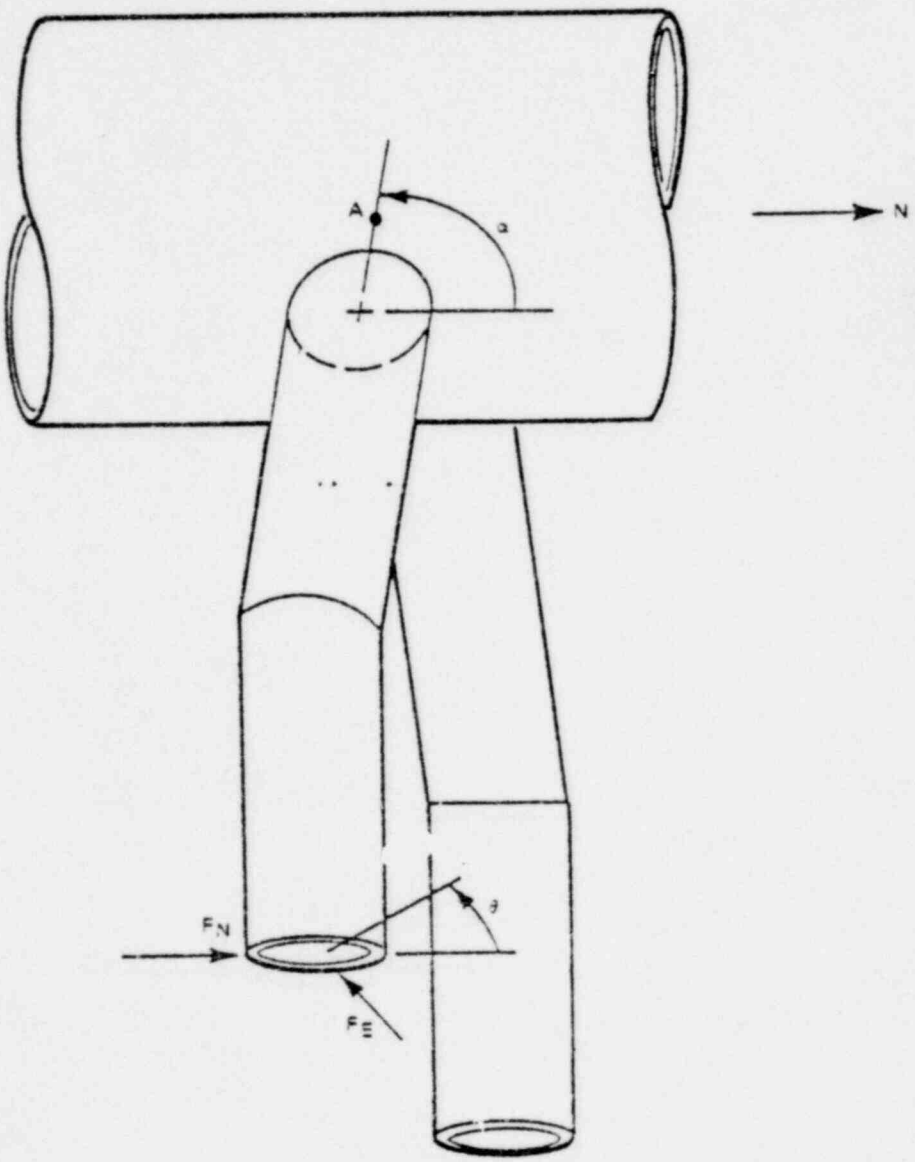

Figure 4-18. Notation Used for Transforming RSEL Reversals into Stress Reversals at a Fatigue Evaluation Location A

5. REFERENCES

1. Mark I Containment Program Load Definition Report, (NEDO-21888).

2. Full Scale Test Program Final Report, (NEDO-24539).

3. H. O. Fuchs, D. V. Nelson, M. A. Burke, and T. L. Toomay, Shortcuts in Cumulative Damage Analysis, Society of Automotive Engineers, Paper No. 730565, 1973.

4. D. V. Nelson and H. O. Fuchs, Predictions of Cumulative Fatigue Damage Using Condensed Load Histories, Society of Automotive Engineers, Paper No. 750045, February 1975.

5. J. M. Biggs, Introduction to Structural Dynamics, McGraw-Hill Book Company, 1964.

6. E. C. Rodabaugh and I. J. Atterbury, Phase Report No. 3 on Flexibility of Nozzles in Cylindrical Shells, Contract No. W- 405-eng-42, Task 16, to USAEC, Battelle Memorial Institute, Columbus, Ohio, December 22, 1967.

APPENDIX A

STATIC CALIBRATION TESTS PERFORMED ON THE DOWNCOMERS OF THE FULL SCALE TEST FACILITY

1. TEST SCHEDULE

Six downcomer bending bridge strain gage calibration tests were performed by Wyle Laboratories[1] involving a pushing or a pulling between downcomer number 5, 6, 7 and 8 of the Full Scale Test Facility (FSTF). The test sequence is given in Table 1. The objective of these tests was to determine load/strain transformation coefficients for downcomer numbers 6 and 8 to be used in the methodology for defining downcomer lateral loads.

2. EQUIPMENT

2.1 Calibration Assembly

The forces required to generate the bending moments were generated by a specially designed calibration assembly. This assembly consisted of a calibration fixture, some miscellaneous parts and four cross assemblies which were welded in place in the downcomers. Each cross assembly had a pin located at its center to which one end of the calibration fixture was attached. The center pin on the cross assembly in the other test downcomer was attached to an auxiliary piece which connected to a dynamometer. The other end of the dynamometer was connected through a screw assembly to the calibration fixture. The nut on the screw assembly could then be turned to manually apply the load. The dynamometer was installed in an in-line position with the force such that it was held in tension for both push and pull tests. Figures 1 and 2 illustrate the use of the calibration assembly.

2.2 Instrumentation

2.2.1 Displacement Gages

Downcomer displacement was measured using a Kafar displacement gage which has a range of 0-1 inch with an accuracy of ± .001 inch. The displacement gages were mounted independent of the downcomers and the load application fixtures. Figure #3 illustrates how the displacement gages were mounted.

(1) Wyle Laboratories Final Data Report for the Recalibration of the Downcomer Strain Gages, Report No. 26298-14, September 29, 1978.

2.2.2 Dynamometer

An F.A. Dillon Co. force gage, calibrated over a 0-2500 lb. range, accurate to ± 25 lbs., was used to measure the force increments applied to the downcomers. The positioning of the force gage for the two types of tests is shown in Figures 1 and 2.

2.2.3 Strain Gages

Downcomer numbers 6 and 8 are instrumented with full bridge strain gages located on cross axes for the measurement of bending stresses. In addition to the full bridge gages there are eight uniaxial strain gages, located at the intersection of downcomer No. 6 and the vent header, lying in a pattern of one every 45 degrees (beginning top dead center) around the circumference of the downcomer. There are eight additional gages located in a similar manner around downcomer No. 8.

These full bridge and uniaxial strain gages are comprised of Ailtech Model SG-158 weldable strain gages which are temperature compensated to a temperature of 650°F. The uniaxial gages were monitored to insure that stresses did not exceed yield in the region of the downcomer attachment to the vent header shell.

Sign conventions for the bending bridges were north and east, positive output; south and west, negative output.

2.2.4 Data Acquisition System

Data acquisition was accomplished using a Varian V77-600 minicomputer and a NEFF system 620 signal conditioning and amplification system.

3. CALIBRATION PROCEDURE

The calibration assembly was installed and the test sequence summarized in Table 1 was started. Each test consisted of three unrecorded shakedown cycles followed by two recorded cycles. Each cycle consisted of loading the downcomers in 300 lb. increments up to 2400 lbs. and then unloading in 300 lb. increments

back to zero lbs. The loads were applied in a smooth, even, continuously increasing or continuously decreasing manner and were held constant during data acquisition.

A computer listing of all bending bridge and uniaxial gages was made at each force increment for all tests. These listings comprise the only test record of strain gage data. Data for the Dillon force gage and the displacement gages were recorded on data sheets by test personnel inside the wetwell.

4. TEST RESULTS

4.1 Linearity

Linearity was excellent on the force vs displacement plots with a correlation greater than .99 on the lines established by linear regressions on the test data.

Linearity was also excellent on the force vs bending strain plots for the primary bending bridges (bridges oriented in the plane of the applied force). Linearity was evident, though not as pronounced, for strain data from the bending bridges transverse to the direction of the applied force.

4.2 Repeatability

The data demonstrated a high degree of repeatability. Examination of the plots showed the patterns followed by the data during the first cycle, with few exceptions, were seen in the second cycle plots.

4.3 Data Consistency

Displacement and bending bridge data correlated well, with the higher bending strains indicative of the greater displacement.

4.4 Hysteresis Effects

Little hysteresis was observed in displacement and primary bending strain data. The hysteresis in the transverse bending strain data was usually greater than that for the primary bending strain data.

4.5 Push-Pull Comparisons of Downcomer Numbers 6 and 8

The data displayed in the push-pull comparison curves was derived from actual test data by taking the averages of the data points for each cycle in the test of interest. Slopes are derived by taking a linear regression on the actual data points. Slope magnitudes were, in general within 3% of one another for the corresponding push and pull tests. Typical results are provided in Figure 4 for Tests No. 3 (pull test) and No. 6 (push test) conducted on downcomer number 6.

Downcomers No. 6 and No. 8 exhibited a similar value of stiffness in the axial direction. A comparison of the stiffness in the radial direction indicated that downcomer No. 8 is about 14% stiffer than downcomer No. 6.

Table 1

SUMMARY OF PUSH/PULL CALIBRATION TESTS PERFORMED ON THE FSTF DOWNCOMERS

Test Sequence	Test No.	Test Type	D/C Pair
1	1	Pull	5 & 6
3	2	Pull	7 & 8
6	3	Pull	6 & 8
5	6	Push	6 & 8
2	7	Push	5 & 6
4	8	Push	7 & 8

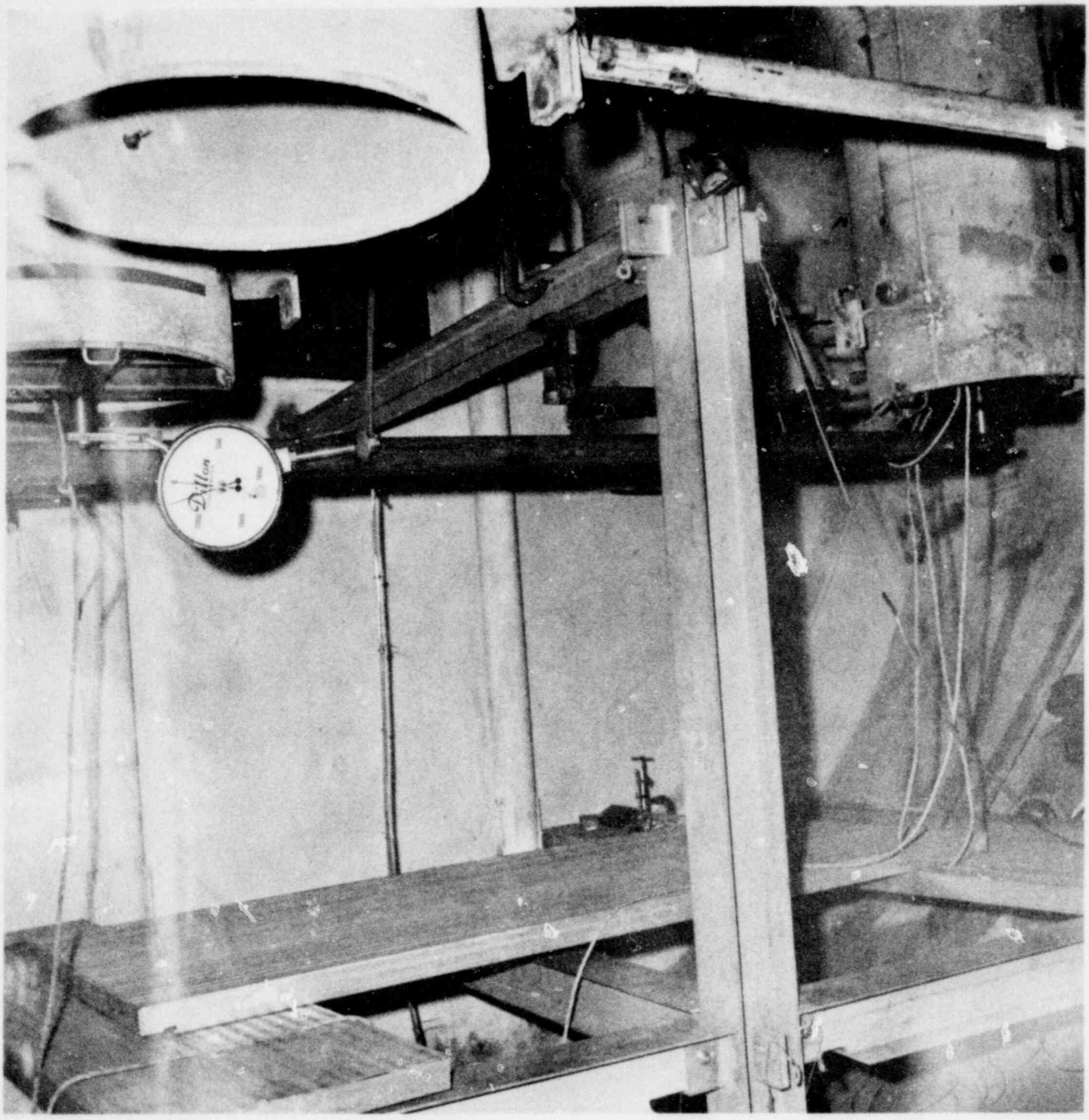

Figure 1. Calibration Assembly Arrangement Pull Test

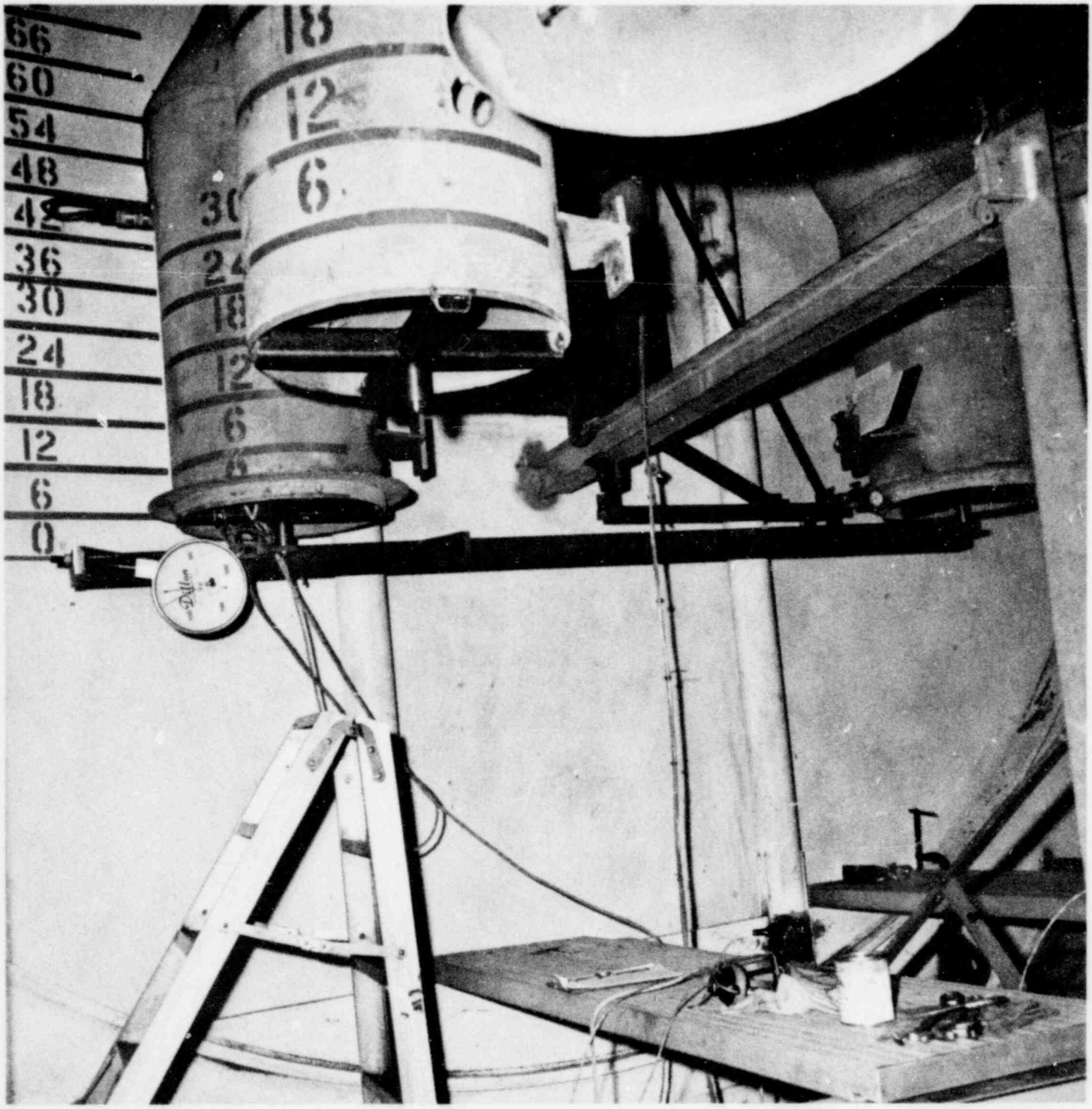

Figure 2. Calibration Assembly Arrangement Push Test

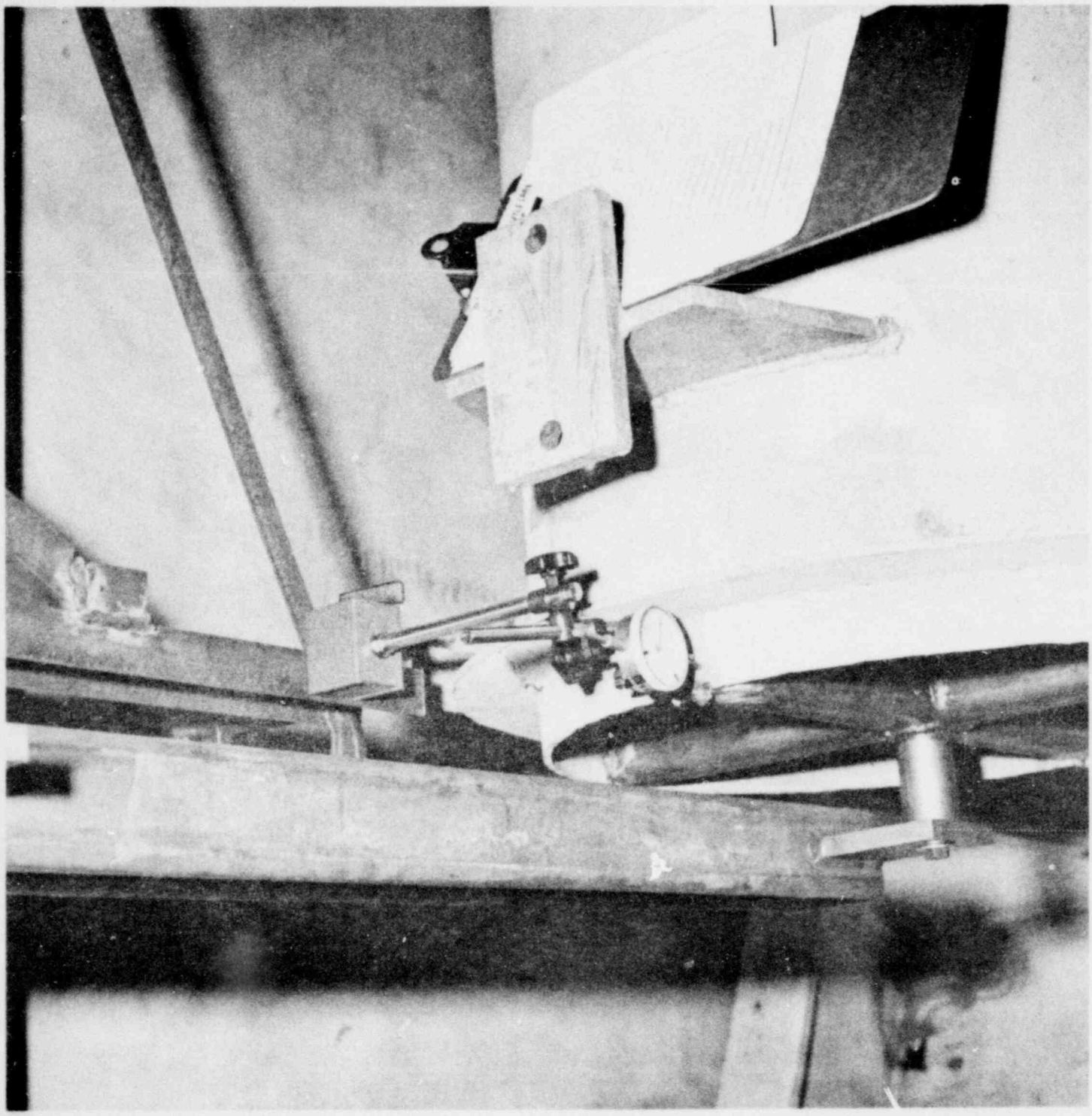

Figure 3. Fixture for Positioning Displacement Gage

*

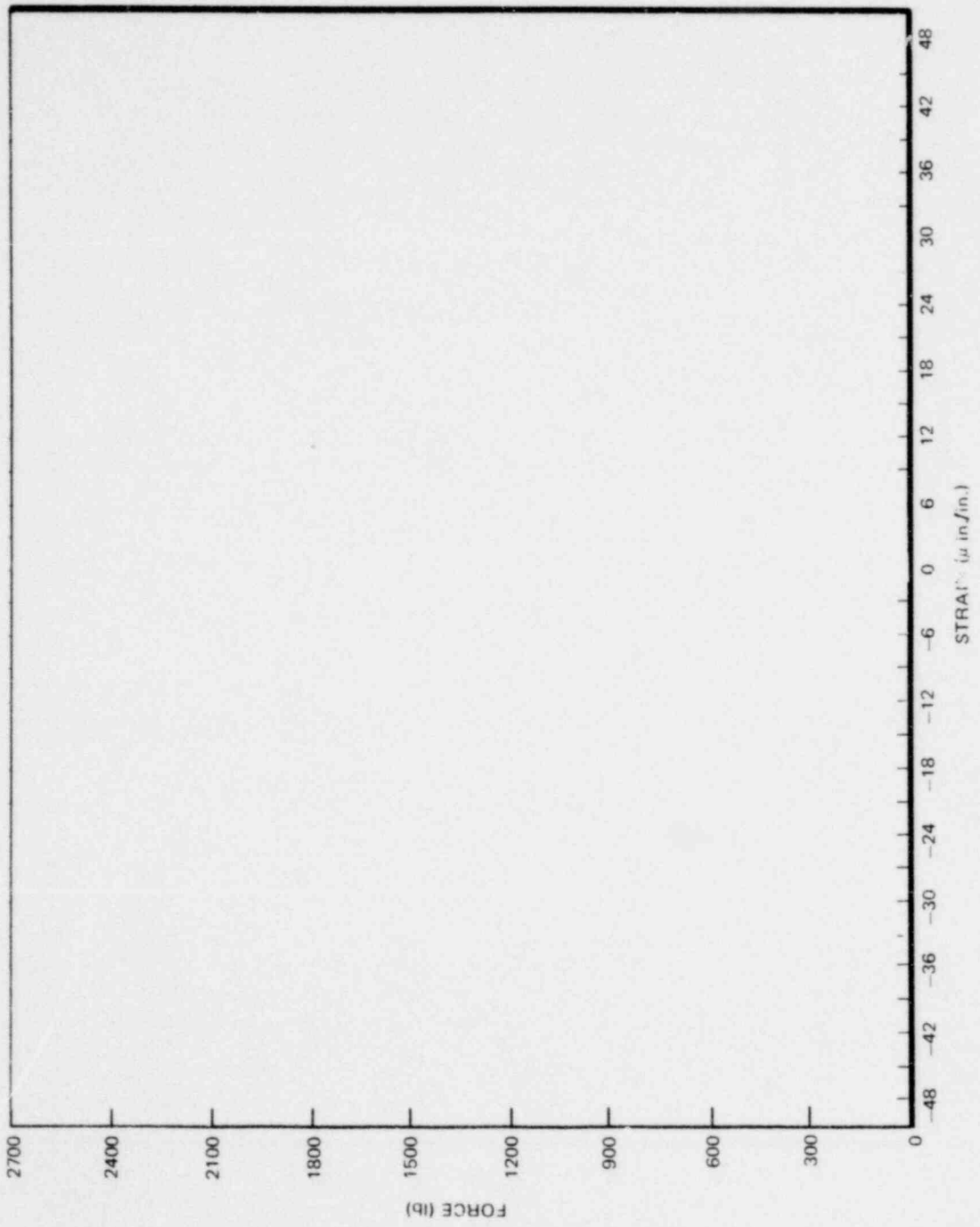

Figure 4. Comparison of Test No. 3 and No. 6 Pull/Push Tests on Downcomer 6
*Proprietary information deleted

APPENDIX B

CALCULATION OF ROTATIONAL STIFFNESS CONSTANTS FOR FULL SCALE TEST FACILITY DOWNCOMERS

The dimensions of the FSTF downcomer/vent header system, which basically correspond to the Monticello plant geometry, except for a shorter downcomer, are given in Figure 1. The downcomer can be assumed rigid with respect to the flexible downcomer/vent header junction. The downcomer/vent header system can therefore be modeled as a rigid downcomer with a rotational spring at the boundary, as shown in Figure 1 (b). For a rotation (θ) of the downcomer about the junction in the East-West direction, the rotational displacement (ϕ) at the end of the downcomer is

$$\phi = \theta \ell \tag{1}$$

where ℓ is the radial distance from the junction to the downcomer end. The corresponding lateral displacement (δ) to the rotation (θ) is

$$\delta = \delta' \cos \alpha \tag{2}$$

where the angle (α) is as shown in Figure 1(b). If a load (F) is applied in the East-West direction to the end of the downcomer, the resulting moment (M) at the downcomer/vent header intersection is

$$M = F\ell \tag{3}$$

where ℓ is the vertical distance from the junction to the downcomer end. The moment (M) can also be expressed as

$$M = k_1 \theta \tag{4}$$

where k_1 is the rotational stiffness of the downcomer/vent header junction in the East-West direction.

Equating Equations (3) and (4), we have

$$F\ell' = k_1\theta = k_1 \frac{\delta'}{\ell} = k_1 \frac{\delta}{\ell \cos \alpha}$$

or

$$F = k_1 \frac{\delta}{\ell' \ell \cos \alpha} \tag{5}$$

but F can also be expressed as

$$F = k_{ew} \delta \tag{6}$$

where k_{ew} is the force required to produce a unilateral displacement of the downcomer end in the East-West direction. The average translational stiffness k_{ew} for FSTF downcomer 6 is 1,828 lb./in. Using Equations (5) and (6) and the FSTF dimensions, the rotational FSTF junction stiffness k_1 in the East-West direction can be determined as

$$k_{ew} = \frac{k_1}{\ell' \ell \cos \alpha}$$

or

$$k_1 = k_{ew} \ell' \ell \cos \alpha \tag{7}$$

$$k_1 = (1828 \text{ lb/in}) (93.35 \text{ in}) (97.42 \text{ in}) \cos (16.61°)$$

$$k_1 = 1.593 \times 10^7 \text{ in-lb/rad}$$

In order to determine the rotational stiffnesses of other Mark I plant downcomer/vent header junctions in the East-West direction, the general relationship is used for the rotational stiffness (k_r) at a junction

$$k_r \alpha \frac{\pi E d^2 t_2}{8} \left[\left(\frac{T}{D} \right)^{3/2} \left(\frac{T}{t_2} \right) \left(\frac{D}{d} \right) \right] \tag{8}$$

where α indicates proportionality and the other variables are defined as shown in Figure 1.

Since k_1 is known from the calibration tests, it is possible to determine the proportionality constant (C) of Equation (8) as follows:

$$k_1 = 1.593 \times 10^7 \text{ in-lb/rad} = \frac{C \times \pi E d^2 t_2}{8}\left[\left(\frac{T}{D}\right)^{3/2}\left(\frac{T}{t_2}\right)\left(\frac{D}{d}\right)\right]$$

or

$$C = \frac{(8)(1.593 \times 10^7 \text{ in-lb/rad})}{\pi E d^2 t_2}\left[\left(\frac{T}{D}\right)^{3/2}\left(\frac{T}{t_2}\right)\left(\frac{D}{d}\right)\right]^{-1}$$

Using the FSTF dimensions given in Figure 1, and assuming the elastic modulus E to be 30×10^6 psi, the proportionality constant (C) is determined to be 13.901. Equation (8) can now be used to determine a generic relationship for the rotational stiffness (k_1) of all downcomer/vent header junctions in the East-West direction.

$$k_1 = \frac{13.901\pi}{8} Ed^2 t_2\left[\left(\frac{T}{D}\right)^{3/2}\left(\frac{T}{t_2}\right)\left(\frac{D}{d}\right)\right]$$

or

$$k_1 = 5.46\, Ed^2 t_2\left[\left(\frac{T}{D}\right)^{3/2}\left(\frac{T}{t_2}\right)\left(\frac{D}{d}\right)\right] \quad (8)$$

Referring back to Equation (7), a similar relationship for the rotational stiffness (k_2) in the North-South direction could be derived as

$$k_2 = k_{ns} L'^2 \cos\alpha \quad (9)$$

where k_{ns} is the translational stiffness of the downcomer in the North-South direction and the other terms are as previously defined in Figure 1. Using Equations (2) and (9) the ratio between the junction stiffness in the East-West and North-South directions is

$$\frac{k_2}{k_1} = \frac{k_{ew}\, \ell' \ell \cos \alpha}{k_{ns}\, \ell' \ell \cos \alpha} = \frac{k_{ew}}{k_{ns}} \qquad (10)$$

Using Equation (10) and an average translational stiffness k_{ns} of 10,527 lb/in determined from push/pull calibration tests conducted by Wyle Laboratories (Appendix A) on instrumented FSTF downcomer number 6, as summarized in Figures 2 and 3.

$$\frac{k_2}{k_1} = \frac{10,527}{1,828} = 5.76$$

Therefore, the rotational stiffness (k_2) of the Mark I plant downcomer/vent header junctions in the North-South direction can be determined by scaling the stiffness value (k_1) determined from Equation (8) for the East-West direction as

$$k_2 = 5.76\, k_1 \qquad (11)$$

The push/pull calibration test results on the instrumented FSTF downcomer number 8 are shown in Figures 4 and 5. The downcomer/vent header junction stiffnesses determined for downcomer number 6 were selected for use in the load definition. These were considered representative since downcomer 8 junction stiffnesses were of similar magnitude.

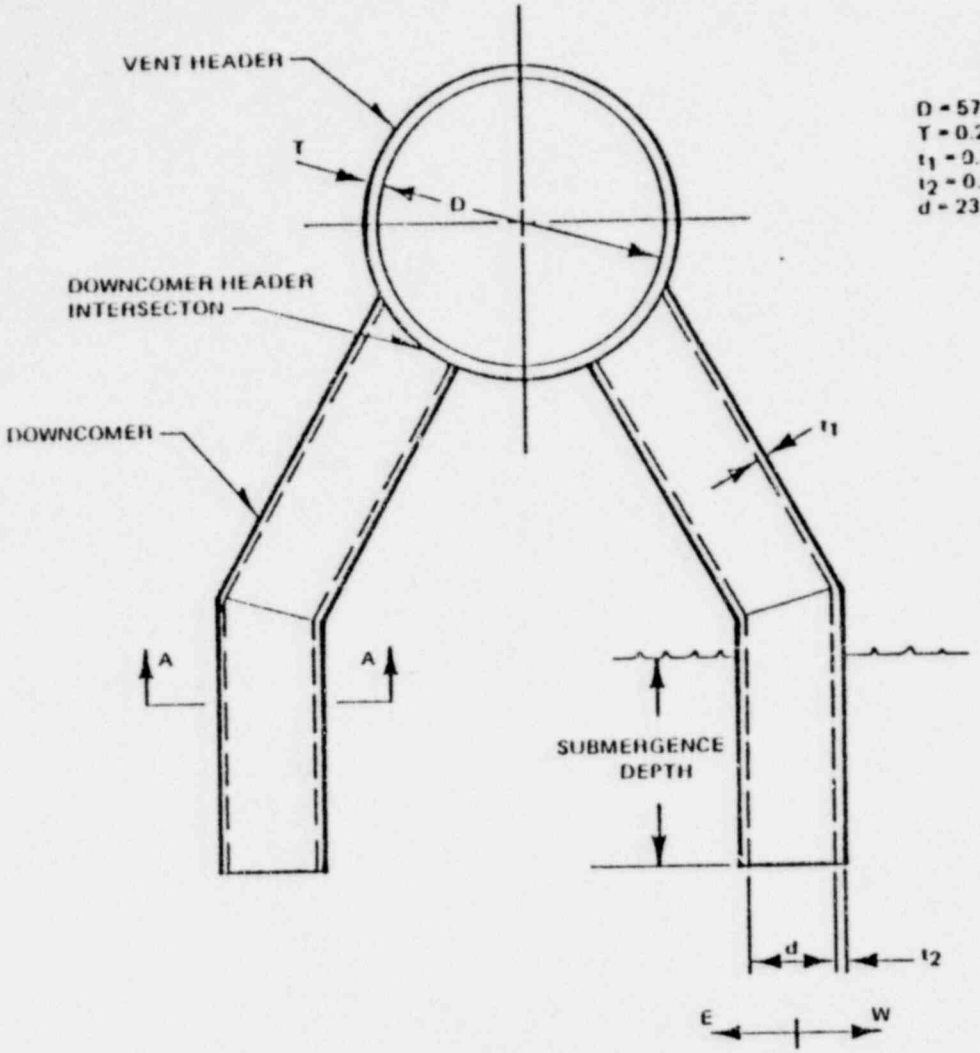

FIGURE 1 (a)

D = 57 in.
T = 0.25 in.
t_1 = 0.375 in.
t_2 = 0.25 in.
d = 23.5 in.

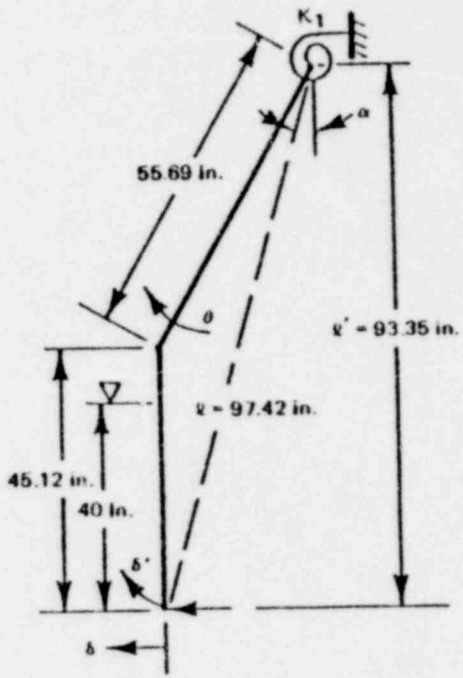

FIGURE 1 (b)

Figure 1. Typical Downcomer/Vent Header Structure Showing Both General and FSTF Dimension Idealized as a Single Degree of Freedom

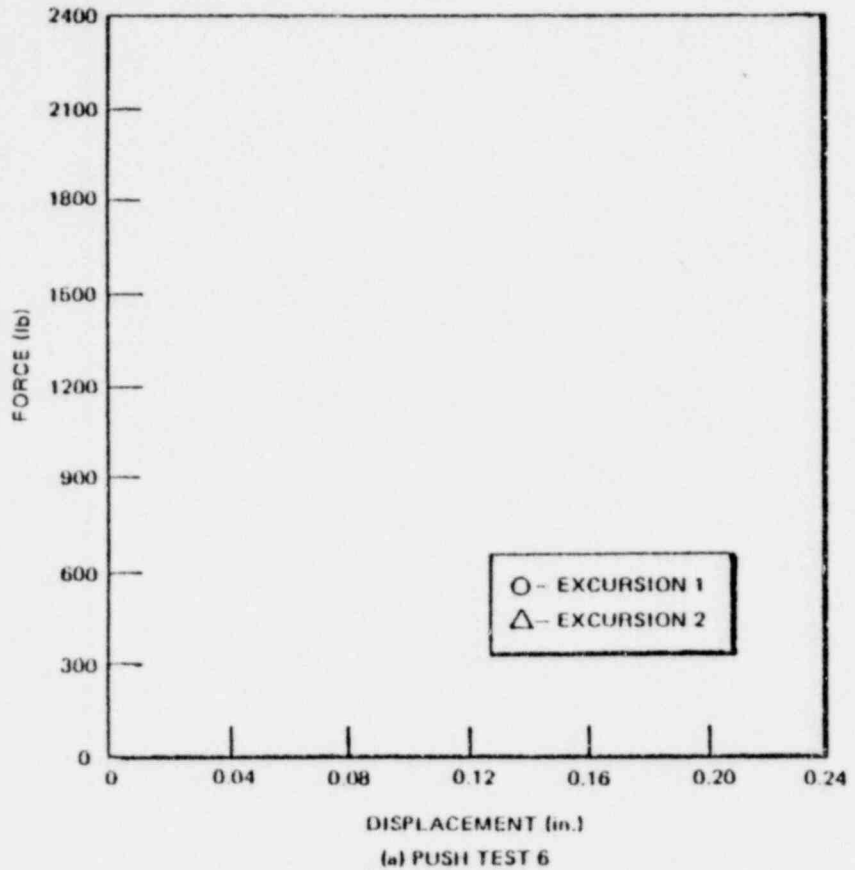

(a) PUSH TEST 6

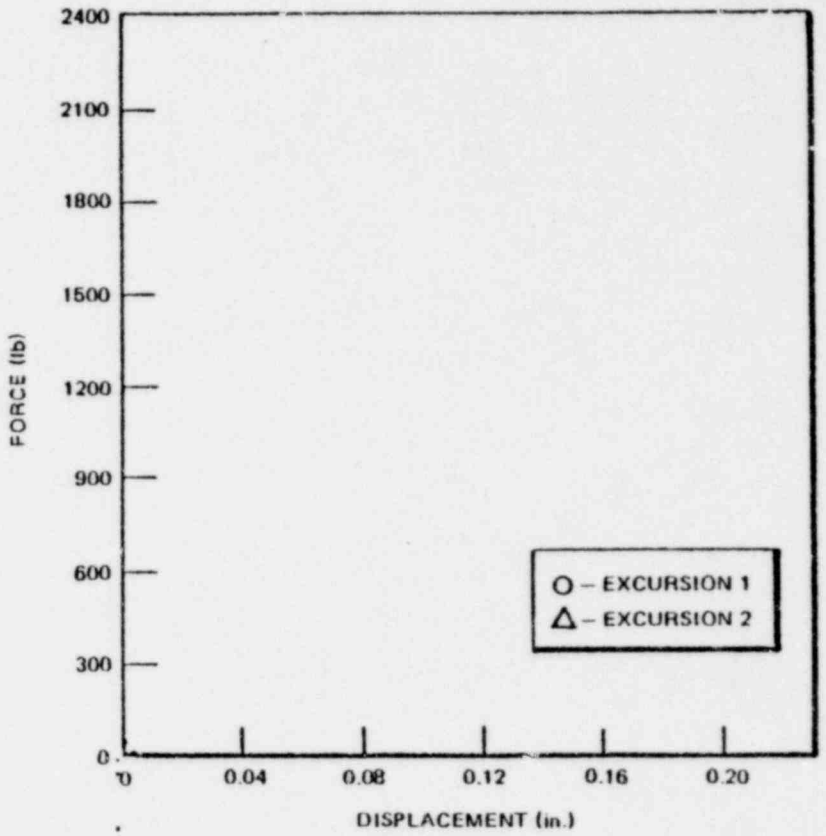

(b) PULL TEST 3

Figure 2. Final Wyle Push/Pull Calibration Tests on Downcomer 6 in the North-South Direction

*Proprietary information deleted

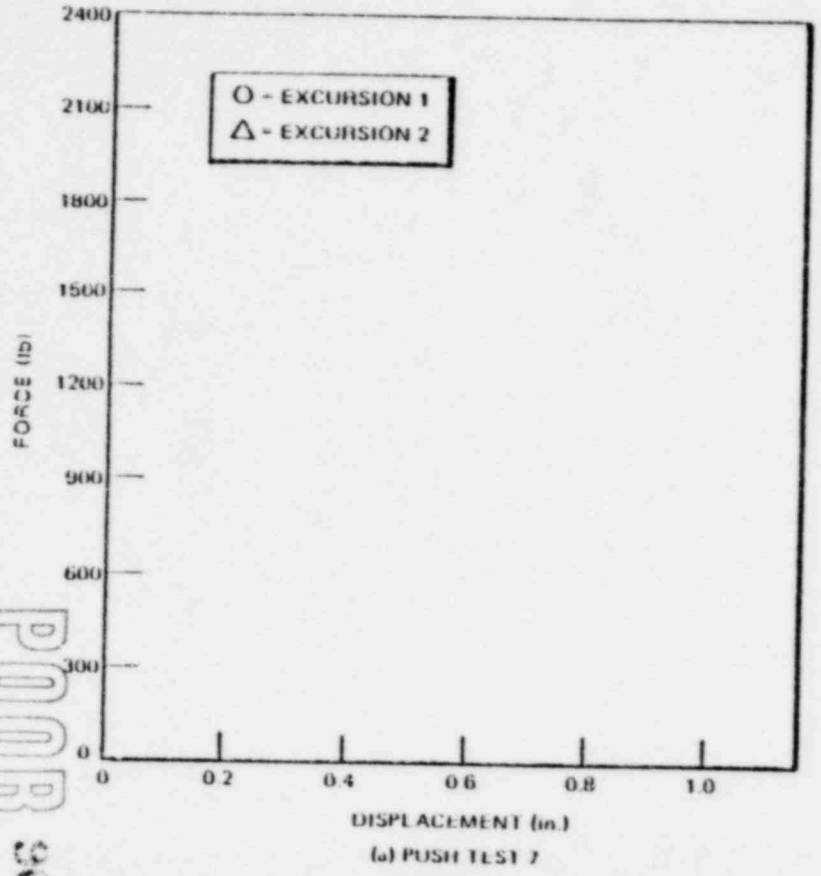

(a) PUSH TEST 7

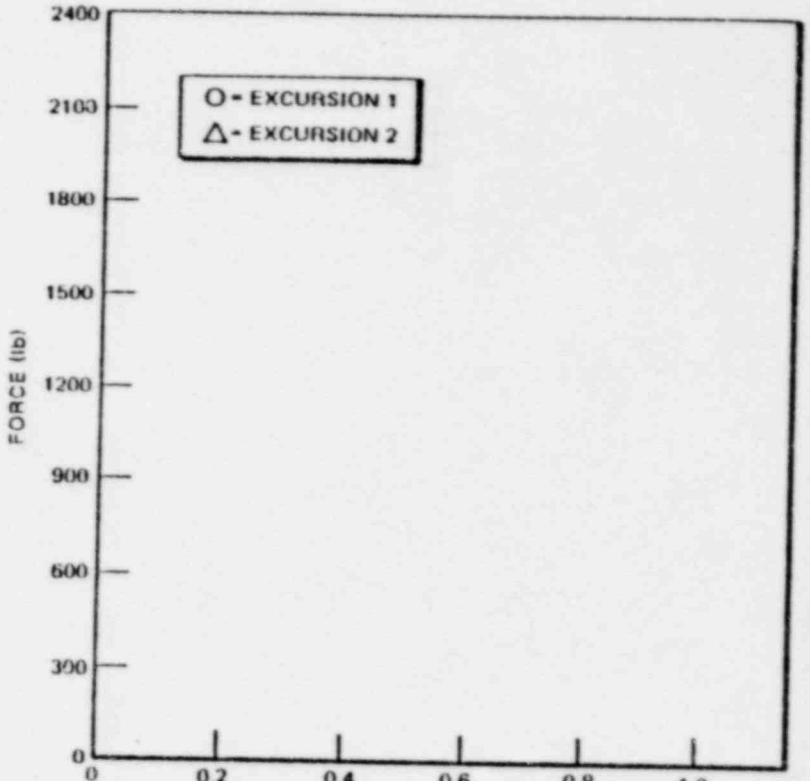

(b) PUSH TEST 1

Figure 3. Final Wyle Push/Pull Calibration Tests on Downcomer 6 in the East-West Direction

*Proprietary information deleted

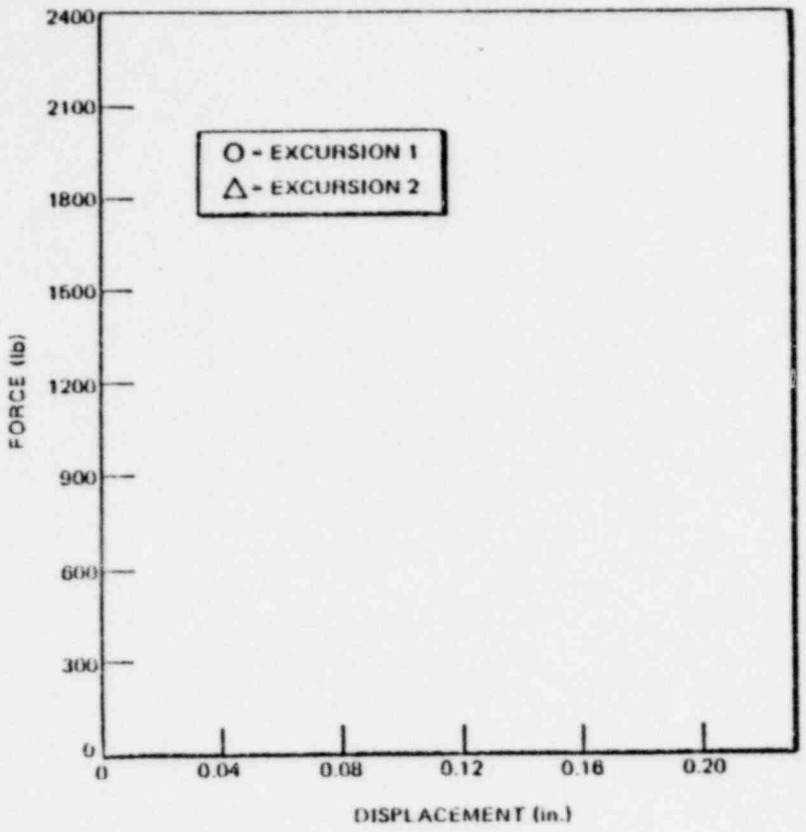

(a) PUSH TEST 6

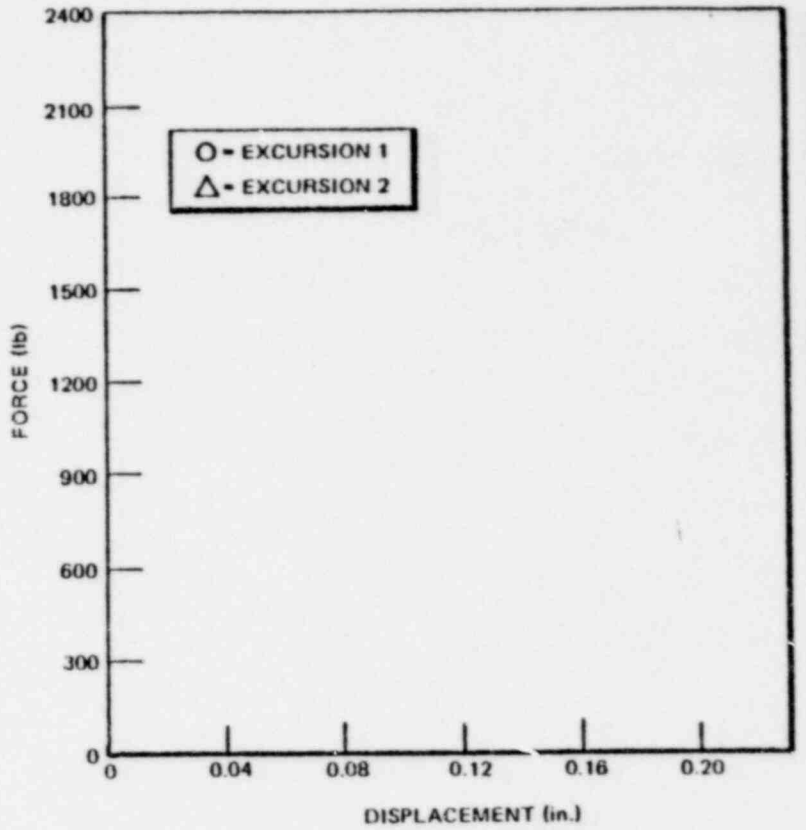

(b) PULL TEST 3

Figure 4. Final Wyle Push/Pull Calibration Tests on Downcomer 8 in the North-South Direction

*Proprietary information deleted

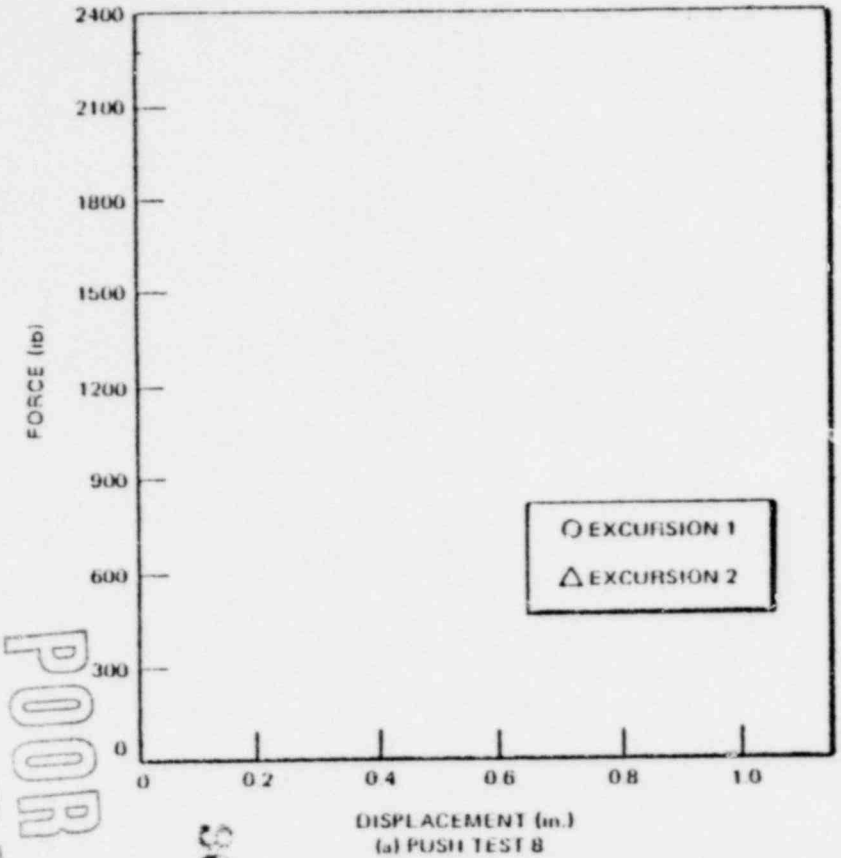

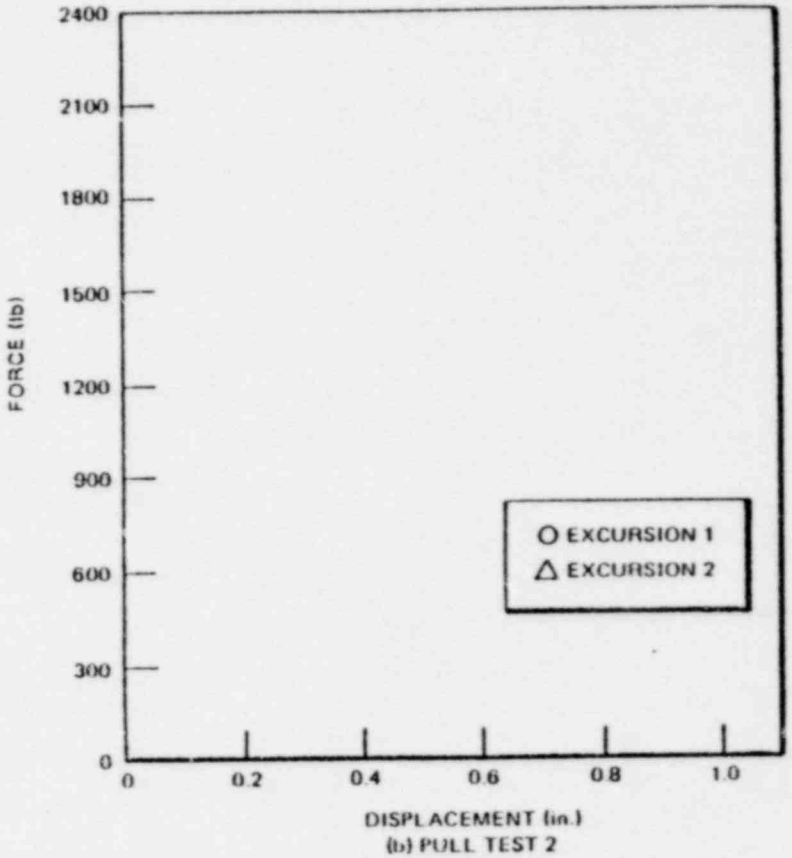

Figure 5. Final Wyle Push/Pull Calibration Tests on Downcomer 8 in the East-West Direction

*Proprietary Information deleted

NUCLEAR ENERGY DIVISIONS • GENERAL ELECTRIC COMPANY
SAN JOSE, CALIFORNIA 95125

GENERAL ELECTRIC

TECHNICAL INFORMATION EXCHANGE

TITLE PAGE

AUTHOR	SUBJECT 730	TIE NUMBER 79NED90
		DATE August 1979
TITLE Mark I Containment Long Term Program - Development of Downcomer Lateral Loads from Full Scale Test Facility Data - Task Number 7.3.2		GE CLASS I
		GOVERNMENT CLASS --
REPRODUCIBLE COPY FILED AT TECHNICAL SUPPORT SERVICES, R&UO, SAN JOSE, CALIFORNIA 95125 (Mail Code 211)		NUMBER OF PAGES 81

SUMMARY

This document provides the methodology for definition of the hydraulic loads produced on the Mark I pressure suppression containment untied downcomers during a postulated loss-of-coolant accident. Resultant static equivalent lateral loads are provided for the air clearing, condensation oscillation and chugging regimes of the postulated event. This document has been prepared for the Mark I Owners as part of the Mark I Containment Program.

This document was prepared by EDS Nuclear Inc. for General Electric Company.

By cutting out this rectangle and folding in half, the above information can be fitted into a standard card file.

DOCUMENT NUMBER NEDO-24537

INFORMATION PREPARED FOR Nuclear Power Systems Division

SECTION Containment Improvement Programs

BUILDING AND ROOM NUMBER PYD 409 MAIL CODE 905

GENERAL ELECTRIC